Robotica (2018) volume 36, pp. 738–766. © Cambridge University Press 2018
doi:10.1017/S0263574718000024

Kinematic calibration of serial manipulators using Bayesian inference

Elie Shammas* and Shadi Najjar

Department of Mechanical Engineering and Department of Civil and Environmental Engineering American University of Beirut, Beirut, Lebanon. E-mail: sn06@aub.edu.lb

(Accepted December 30, 2017. First published online: January 25, 2018)

SUMMARY

In this paper, a new calibration method for open-chain robotic arms is developed. By incorporating both prior parameter information and artifact measurement data, and by taking recourse to Bayesian inference methods, not only are the robot kinematic parameters updated but also confidence bounds are computed for all measurement data. In other words, for future measurement data not only the most likely end-effector configuration is estimated but also the uncertainty represented as 95% confidence bounds of that pose is computed. To validate the proposed calibration method, a three degree-of-freedom robotic arm was designed, constructed, and calibrated using both typical regression methods and the proposed calibration method. The results of an extensive set of experiments are presented to gauge the accuracy and utility of the proposed calibration method.

KEYWORDS: Kinematic calibration; Bayesian updating; Likelihood function; Second-moment Bayesian method.

Nomenclature

$\varphi, \bar{\varphi}, \tilde{\varphi}$	Nominal, actual, and deviation of the kinematic parameters
l	The length of the parameter vector φ
θ, η	Inter-link joint angle and resolver or encoder reading (converted to angles)
m	Number of measurements
p	Position of the origin of the end effector coordinate frame
L_{ab}, l_{ab}	Artifact actual and predicted length between points a and b
μ, Σ, ρ	Mean vector, co-variance matrix, and correlation matrix
$\mathcal{L}, \ell$	Likelihood function and its natural logarithm

1. Introduction

At a basic level, kinematic calibration can be thought of as a system identification problem. More precisely, given a robotic manipulator with an assumed kinematic model, a nominal set of parameters, and a set of measurements, kinematic calibration computes the deviations of the kinematic parameters from their nominal values to improve the absolute positioning accuracy of the manipulator's end-effector. During manufacturing and assembly of a robotic arm, one could possibly reduce the deviations from the nominal values. Nonetheless, without a final calibration procedure, the accuracy of the manipulator can neither be improved nor assessed. In fact, similar to fingerprints in humans, each robotic arm will have its own unique set of kinematic parameters even if it belongs to the same family of robots. This is referred to as an "arm signature" which in turn necessitates the kinematic calibration procedure.[6]

An important aspect of calibration is the assumed kinematic model of the robotic arm. Extensive research has been conducted to identify the most suitable kinematic models for robotic arms. A metric used to compare various models is completeness, which evaluates the arm's capability to

* Corresponding author. E-mail: es34@aub.edu.lb

capture deviations of the kinematic parameters continuously and uniquely while utilizing the smallest set of parameters.[23] One of the most commonly used kinematic models for open-chain robotic arms is the one devised by Denavit–Hartenberg in refs. [9,19]. This model exhibits singularity for robotic arms that have almost parallel consecutive joint axes.[48] Accordingly, the *generalized* D-H convention was proposed to overcome this singularity at the cost of appending the kinematic parameters set by an additional parameter per joint.[21] Alternatively, researchers proposed using a "complete and parametrically continuous" model for parameter identification namely the Product-Of-Exponential formula to eliminate redundancy of the kinematic parameters in the error models as was respectively shown in refs. [22,23,44,56]. Edwards and Galloway[13] developed a calibration method that required a single point measurement whereas[40] devised a method that uses articulated single point measurement. Along the same lines,[4,18] and[8] proposed methods that gauge the quality of potential measurement configurations. Other calibration methods involved more elaborate measurements of the end-effector either by using dedicated instrumentation or other measurement machines.[34,43]

It is worth noting that all the above models, being kinematic in nature, capture structural deviations from nominal values that are due to physical imperfections such as assembly errors, encoder zero versus robot home position (encoder offsets), joint axes misalignment, and manufacturing tolerances.[33] However, other kinds of errors are not captured by kinematic models such as joint non-rigidity, encoder advance and retard error, axis wobble, and temperature and humidity effects as depicted in refs. [12,30,33,54]. The first family of errors pertaining to the kinematic models is typically referred to as "geometric" errors whereas the second family of errors is labeled as "non-geometric" errors. It is worth noting that "non-geometric" errors could account to up to 10% as was stated in ref. [46]. An analysis of the number of errors to be identified versus the number of required measurements in the context of manipulator calibration is presented in refs. [35,36]. It should be noted that error modeling is an integral part of designing robust controllers for robotic arms. In ref. [55], dynamic modeling and re-parametrization were used to design a hybrid controller for a robotic arm that maintains accuracy and joint convergence speed performance in the presence of disturbance due to variations of the payload.

In addition to the possibility of using various kinematics models, there are various calibration methods that could be adopted. The commonality among all calibration methods is the usage of a measurement process that either uses another measuring machine or an artifact with known relevant attributes. For instance, the end-effector location and orientation could be measured via another machine and the acquired information is used to compute the kinematic parameters by minimizing an error (or cost) function. In this case, the output of the measuring equipment is used as ground truth. This measurement process could use various modalities such as: visual or computer-aided theodolite systems,[10,33,54] laser-based setups,[1,15,42,45,50] or coordinate measuring machines (CMM) in ref. [11]. Along the same lines, researchers developed calibration methods that utilize an integrated system such as a manipulator and a stereo camera. Such methods calibrate the entire system by identifying the kinematic parameters of both sub-systems as was depicted in ref. [3]. In fact, this integrated method effectively closes the kinematic chain in which the manipulator is a sub-system. The complement of the manipulator could be another mechanical structure which effectively calibrates a closed-kinematic chain or a parallel robot.[14,32] The utility and robustness of such closed-loop calibration approaches were standardized in ref. [25].

Other common methods of calibration depend on the usage of an artifact with known and traceable attributes. Examples of such calibration methods use line constraints in refs. [42, 46] or plane constraints in ref. [28]. The *traceability* of the artifact features refers to the method used to measure these features and how the measurement accuracy can be related to a certified lab or national standard. The calibration method proposed in this paper belongs to the second family and uses a distance constraint between two conic holes similar in nature to methods depicted in refs. [26,37]. This kind of distance constraint is referred to as a "volumetric" measurement.

The work on robot calibration summarized above provides an improved estimate of the kinematic parameters compared to their nominal values. In ref. [31], the Product-Of-Exponential model was used together with a Gaussian Process *regression* to compensate for geometric and non-geometric errors. Nonetheless, a statistical model can be devised such that not only the nominal means of the kinematic parameters are estimated but the uncertainties in these parameters are also quantified. Accordingly, one can define a *prior* statistical model that describes the probability distribution of each of the nominal kinematic parameters. In this paper, a probabilistic calibration method is developed

to *update* the prior knowledge of the statistics of the model parameters using Bayesian inference methods. The updated model, typically referred to as a *posterior* model, not only provides an improved estimate of the kinematic parameters means but also updates their probabilistic distributions, thus, making posterior error analysis possible. Previous work has approached the kinematic calibration of robotic manipulators by taking recourse to such statistical approaches. Namely,[46] and[27] made use of "a priori" knowledge about the kinematic parameters by implementing a "maximum a posteriori" (MAP) estimate. More specifically, in ref. [46], the authors utilized a D-H kinematic model in conjunction with a measuring device that ensures that the end-effector is constrained to move along a straight line to define a likelihood function. Based on geometric errors of the kinematic model and those of the measuring devices, an algorithm based on maximum likelihood was developed to calibrate the model parameters. The method presented in this current paper extends previous work by utilizing Bayesian updating to compute confidence intervals on the measurement errors. While the work presented in ref. [46] aimed at updating the geometric parameters by iteratively maximizing the likelihood function, the Bayesian updating method presented in this paper was employed to update the geometric parameters in a non-iterative approach. Another stark difference is that in this current paper, a "passive" artifact (plate with conic holes) was used to calibrate the robot rather than using another machine that has its own geometric and non-geometric errors.

In this paper, we shall limit the analysis to Cartesian Measuring Machines, a particular family of robotic arms that only have encoders at the joint and no actuators. Such machines are used in metrology applications where a technician articulates the robotic arm to do the measurements. Nonetheless, the calibration method presented in this paper could be adapted to calibrate robotic manipulators by adding geometric and non-geometric errors associated with actuators such as gear backlash and shaft flexing. This paper is organized as follows. In Section 2, kinematic calibration is introduced along with all the relevant background information such as kinematic models, kinematic parameters, and calibration artifacts. In Section 3, typically regression-based calibration methods are presented along with well-defined error and cost functions. The novel calibration method developed in this paper is presented in Section 4 where the problem is formulated in the Bayesian inference framework, the statistical characteristics of the model parameters are updated, and confidence bounds for the predicted lengths are defined. In Sections 5 and 6, the details of the design and construction of the three degree-of-freedom robotic arm and an extensive set of experiments to evaluate the proposed calibration method and to compare it to conventional calibration approaches are, respectively presented. A discussion of the results is presented in Section 7 and concluding remarks are left to Section 8. Finally, supporting material such as the formulation of maximum likelihood calibration, the equivalence of regression and maximum likelihood calibration methods, and the raw encoder data used for calibration are depicted, respectively, in AppendicesA through C.

2. Kinematic Calibration

At the core of the kinematic calibration of robotic manipulators is devising a procedure that identifies the parameters of a proposed kinematic model. Such a model is utilized to best capture the absolute position and orientation of the end-effector given the kinematic parameters and a set of internal joint configurations. As mentioned in Section 1, this paper does not concentrate on finding the best kinematic model but rather on developing a calibration method to improve the accuracy of a robotic manipulator by focusing on finding the "best" set of kinematic parameters and characterizing their probability distributions.

In this paper, a robust kinematic model for the manipulator is assumed. Moreover, the adopted methodology only considers open kinematic chains which are robotic arms that are comprised of serially connected rigid links. Without loss of generality, it can be assumed that the links are connected via revolute joints. Typically, a transducer is assembled within each joint to measure the relative motion between the adjacent rigid links.

A kinematic model for such an open chain manipulator typically consists of two levels (as was shown in ref. [48]). Level-1 relates the joint's transducer reading to the actual inter-link joint angle, whereas level-2 computes the end-effector pose given the joint angles and the kinematic parameters. Both levels require their own set of parameters. For instance, letting η be a set of transducer or encoder output readings, typically voltage signals, and θ be the set of actual joint angles, one can use a set of

https://doi.org/10.1017/S0263574718000024 Published online by Cambridge University Press

parameters, γ, to relate the two such that

$$\theta = h(\eta, \gamma). \tag{1}$$

This level-1 model could possibly capture geometric errors such as joint offset and signal scaling; however, in many cases, the encoders output angles directly where γ will be a single angular offset parameter that captures the missalignment between the encoder's zero and the home configuration of the joint. Having computed the joint angles, the generalized D-H convention proposed in ref. [21] could be used to construct a level-2 kinematic model. Letting ϕ be a set of kinematic parameters, one can compute the end-effector pose[(1)], x, using the forward kinematic map, f, given by

$$x = f(\theta, \phi). \tag{2}$$

In this paper, the end-effector orientation is ignored, thus setting $x(= p)$ as a three-dimensional vector representing the position of the end-effector. Recall that using the generalized D-H convention, coordinate frames are attached to all the individual links such that the transformation from the base coordinate frame to the end-effector coordinate frame is computed by multiplying the adjacent inter-link transformations in the right order. Accordingly, it suffices to enumerate a set of well-defined kinematic parameters between consecutive links to be able to construct the kinematic model of a robotic manipulator. Since the generalized D-H convention requires *four* parameters per joint, an n-joint robotic manipulator would require $4n$ level-2 parameters.

Moreover, neglecting the electronics and signal noise of encoders and assuming that the encoders' output captures the relative joint rotation, a level-1 model would only require a single offset angle correction parameter per joint. This offset captures the misalignment between the encoder zero position and the manipulators assumed home position. Thus, for the entire kinematic model, an additional parameter per joint is required. In fact, for such a level-1 model, the additional parameter can be lumped in the generalized D-H model such that each joint requires *five* parameters. Hence, for an n-joint robotic manipulator, $5n$ parameters are required. The kinematic model, thus, can be represented by

$$p = k(\eta, \varphi), \tag{3}$$

where p represents the three-dimensional position of the origin of the end-effector's frame, η represents the joints' encoder readings, and φ represents the combined level-1 and level-2 set of kinematic parameters.

During the design stage, one can identify the *nominal* values of all the kinematic parameters of the robot while during manufacturing and assembly, one could try to maintain these nominal values; Nonetheless, this will require unrealistic part tolerances, complicated and costly assembly methods, and extended manufacturing and testing procedures. Even with such costly procedures, it can not be guaranteed that the values of the kinematic parameters will not deviate from their nominal values. Hence, a robust calibration method must allow for quantification of the deviations of the kinematic parameters. Letting φ represent the nominal kinematic parameters, and letting $\tilde{\varphi}$ represent the deviation of the parameters from their nominal values, the actual kinematic parameters of the assembled robotic arm, $\bar{\varphi}$, are given by

$$\bar{\varphi} = \varphi + \tilde{\varphi}. \tag{4}$$

In this paper, a simple point-to-point measurement on an artifact is used as a basis for the proposed calibration method. Comparing the computed length – through the forward kinematics map – between the two poses of the end-effector and the actual distance between the two points on the artifact gives rise to the so-called volumetric errors.

[(1)]Note that, typically in robotics, $x \in SE(3)$ which is the three-dimensional special Euclidean group. In matrix representation, x is a 4×4 homogeneous matrix such that the top-left 3×3 sub-matrix, R, is an element of the $SO(3)$, the special orthogonal group that represents the orientation of the end-effector's coordinate frame. The top-right 3×1 sub-matrix, p, is an element of $\mathbb{R}^3$ that represents the position of the origin of the end-effector's coordinate frame.

https://doi.org/10.1017/S0263574718000024 Published online by Cambridge University Press

3. Typical Regression Calibration

In this section, the de-facto method of parameter identification for robotic arms, that is the regression analysis, is presented. By placing the end-effector in two countersink holes and recording two measurements, one effectively saves the two encoder readings η_a and η_b. Using the encoder readings and the kinematic parameters, one can compute the locations of the end-effector through the forward kinematics to get $p_a = k(\eta_a, \bar{\varphi})$ and $p_b = k(\eta_b, \bar{\varphi})$. Note that, k is the forward kinematics map capturing both level-1 and level-2 models as shown in (3). Also, note that the actual kinematic parameters, $\bar{\varphi}$, which are related to the nominal parameter values as shown in (4) were used. Since only the nominal values of the parameters, φ, are known, the computed end-effector positions, p_a and p_b, depend on the errors in the kinematic parameter, $\tilde{\varphi}$ which are yet to be solved for.

Using the two end-effector positions, p_a and p_b, one can utilize the Euclidean metric to compute the length between the three-dimensional locations, such that

$$l_{ab}(\tilde{\varphi}) = \sqrt{(p_a - p_b)^T \cdot (p_a - p_b)}. \tag{5}$$

Given that the end-effector was placed in the countersink holes on the artifact, the computed length must match the known artifact length, L^i_{ab}. In other words, one can define volumetric length errors for each pair of end-effector measurements such that

$$\mathrm{err}^i_{ab}(\tilde{\varphi}) = L^i_{ab} - l^i_{ab}(\tilde{\varphi}). \tag{6}$$

For a set of pairs of measurements, one can compute a list of errors, $\mathrm{err}^i_{ab}(\tilde{\varphi}) = L^i_{ab} - l^i_{ab}(\tilde{\varphi})$. Since these errors can be either positive or negative, the RMS sum (RMS) being a sign-invariant sum, is used to combine the contribution of all length errors. For an entire calibration with m pairs of end-effector measurements, the total error, $\mathrm{Err}(\tilde{\varphi})$, is given by

$$\mathrm{Err}(\tilde{\varphi}) = \sum_{i=1}^{m} \left(\mathrm{err}^i_{ab}(\tilde{\varphi})\right)^2 = \sum_{i=1}^{m} \left(L^i_{ab}(\tilde{\varphi}) - l^i_{ab}(\tilde{\varphi})\right)^2. \tag{7}$$

The above computed total error is always a positive number. Thus, calibrating the manipulator is rendered to finding a set of kinematic parameter errors, $\tilde{\varphi}$, that minimizes the total RMS error. In other words,

$$\tilde{\varphi}^{reg} = \mathrm{argmin}\, \mathrm{Err}(\tilde{\varphi}). \tag{8}$$

The above minimization problem is referred to as the *least sum of square minimization* or *regression*.[38] There are readily available numerical algorithms that solve this typical minimization problem. However, it is worth noting that the error or cost function in (7) is *highly* non-linear in terms of its argument, $\tilde{\varphi}$. This is due to the trigonometric functions that are used to represent the forward kinematics of the manipulator in (3).

Another conventional approach for calibrating the kinematic model parameters is based on maximizing the likelihood of observing the set of length data or associated error data. This method is presented in Appendix A and the equivalence of both calibration methods is discussed in Appendix B.

4. Bayesian Updating

Conventional approaches for calibrating the kinematic model parameters (regression and maximum likelihood) lead to an optimal set of model parameters that would best fit the measured data. The main shortcoming of these methods lies in the fact that the use of the optimal set of model parameters results in a deterministic estimate of the predicted lengths and an associated deterministic error in the prediction. Information about the reliability of the length estimates and their associated confidence bounds is lacking. Moreover, the conventional approaches do not account for uncertainties that may exist in the actual estimates of the kinematic model parameters and their impact on the estimated lengths or error predictions.

https://doi.org/10.1017/S0263574718000024 Published online by Cambridge University Press

The novel calibration method that is proposed in this paper aims at overcoming these shortcomings by (1) adopting a fully probabilistic model that characterizes the uncertainty in the length predictions of the robotic arm, and (2) assuming that all parameters to be calibrated are random variables that are characterized by probability distributions. The probabilistic nature of the model length predictions and the kinematic model parameters allows for applying Bayesian updating techniques to calibrate the model parameters and more importantly to associate each resulting length prediction with confidence bounds that fully define the reliability of the prediction.

The flexibility of the method lies in its ability to propagate and combine all the sources of uncertainty that affect the resulting length prediction while maintaining the uniqueness of the individual measurements. In other words, the confidence bounds that will result from this exercise will be unique for each measurement and will depend on the different configurations of the robot, that is, pose and orientation of the end-effector. The proposed probabilistic approach provides a global accuracy assessment of the manipulator and quantifies the uncertainty that is associated with each future measurement that is taken by the manipulator. It is this "live" uncertainty feedback for each measurement that allows the user to achieve better confidence intervals for any future measurement.

The novel calibration procedure is based on the well-known Bayesian inference method that allows for combining prior knowledge about model parameters with a new set of measurements to update the probability distribution of the model parameters. In the analysis, the length of an artifact is represented probabilistically by considering that the length is a random variable with a mean and a standard deviation that are represented by

$$\mu_{l_{ab}}(\tilde{\varphi}) = \sqrt{(p_a - p_b)^T \cdot (p_a - p_b)} \tag{9}$$

$$\sigma_{l_{ab}} = e^{\lambda}, \tag{10}$$

where $p_a = k(\eta_a, \tilde{\varphi})$ and $p_b = k(\eta_b, \tilde{\varphi})$ are the predicted locations of the end-effector which are functions of the encoder readings η_a and η_b and the associated deviations of the kinematic parameters ($\tilde{\varphi}$) that are to be updated. It should be noted that the model parameters ($\tilde{\varphi}$) fully define the mean of the length prediction and that e^{λ} reflects the standard deviation in the predicted length about the predicted mean. The exponential term is used to ensure that the standard deviation is a positive quantity.

As mentioned previously, in the probabilistic model, it is assumed that each kinematic model parameter, $\bar{\varphi}$, is a random variable that is defined by the sum of a deterministic nominal value, φ, and a random deviation from the nominal value, $\tilde{\varphi}$. The deviations, $\tilde{\varphi}$, from the nominal values are assumed to be the random model parameters that are to be updated during the Bayesian exercise while maintaining the same nominal value for any given parameter. Accordingly, the deviations $\tilde{\varphi}$ for the different kinematic model parameters in addition to the model parameter λ (representing $\sigma_{L_{ab}}$) are defined by their means, variances, and covariances.

Prior statistics for these model parameters have to be defined as indicated in the following section. The prior statistics of the model parameters are then updated given the new set of length measurements using Bayes' theorem.

4.1. Prior model

The prior statistics of the model parameters (the deviations of the kinematic parameters from the nominal values) and the prior statistics of the additional parameter, λ, need to be estimated prior to the updating process. Ideally, if a company is producing hundreds of the same model manipulators, one could estimate the means and standard deviation of the kinematic parameters using the regression solutions of such production runs. However, the prior statistics of the model parameters of a manipulator can still be estimated even without such historic data. In this paper, since the kinematic model parameters represent deviations from a nominal value, the prior means of the model parameters could be set to zeros such that

$$\mu_i^{pri} = 0, \text{ for } i = 1, \ldots, l, \tag{11}$$

where l is the number of parameters.

https://doi.org/10.1017/S0263574718000024 Published online by Cambridge University Press

Regarding the standard deviations of the kinematic model parameters, a prior estimate could be computed at the design stage by analyzing part tolerance, assembly procedures, and encoder resolutions. Let σ^{pri} represent a set of standard deviations for the prior kinematic model parameters. For parameters that are associated with encoder angles, a good estimate for the standard deviation is half the encoder's resolution. For a link length parameter, the standard deviation could be estimated by the stacked manufacturing tolerances from either the shop drawings or the actual part inspections.

To complete the prior statistics of the model parameters, the possible correlation between the different pairs of model parameters will need to be determined to fully model the covariance matrix of the parameters. Since the model parameters belong to various families (i.e., rigid link lengths, encoder angles, or measurement errors), one should expect different correlation levels between the different parameter pairs. The sensitivity of the proposed calibration method to various prior correlation assumptions will be assessed in Section 7. However, it will be initially assumed that the random variables representing the parameters are statistically independent. As a result, the correlation matrix will be given by

$$\rho^{pri} = \mathbb{I}^{l\times l}, \tag{12}$$

where $\mathbb{I}^{l\times l}$ is the $l \times l$ identity matrix. Having, defined the prior standard deviations and the correlation structure, one can compute the covariance matrix for the prior model, such that the ij-th element is given by

$$\Sigma_{ij}^{pri} = \rho_{ij}^{pri} \cdot \sigma_i^{pri} \cdot \sigma_j^{pri}, \text{ for } i, j = 1, \ldots, l. \tag{13}$$

4.2. Bayesian updating of model parameters

Bayesian techniques allow for updating the prior distributions of the model parameters given a new set of length measurements. The updated posterior distribution (see Eq. (14)) is generally difficult to evaluate except for some special cases where conjugate priors can be employed. In recent years, several methods have been proposed as practical techniques for evaluating the updated model parameters. Direct integration methods in ref. [7], Monte Carlo Markov Chains methods in refs. [5] and [47], system identification methods in ref. [51], and the first-order second-moment Bayesian method (FSBM) in ref. [17] are examples of methods that could be used for this purpose. Interested readers are referred to[16] for additional details about recent computational techniques for estimating posterior distributions.

In this paper, the FSBM proposed by Gilbert[17] will be used to calibrate the probabilistic model parameters using a set of length measurements of an artifact with a known length. The FSBM was developed to provide a practical Bayesian method for problems with multiple model parameters, large data sets, and various data distributions. The method has been employed in calibrating model parameters for different engineering applications such as in refs. [39,52,53], and [41]. Following the derivation in Gilbert,[17] the FSBM uses Bayes' theorem in (14) to update the probability distribution of the model parameters for a given set of data. Thus, letting

$$f_{\Phi|\epsilon}(\Phi|\epsilon) = \frac{\mathcal{L}(\epsilon|\Phi) f_\Phi(\Phi)}{\int_{-\infty}^{+\infty} \cdots \int_{-\infty}^{+\infty} \mathcal{L}(\epsilon|\Phi) f_\Phi(\Phi) d\Phi_1 \cdots d\Phi_l}, \tag{14}$$

where $f_{\Phi|\epsilon}(\Phi|\epsilon)$ and $f_\Phi(\Phi)$ are the updated (given the new data ϵ) and prior joint distributions of the model parameters Φ, $\mathcal{L}(\epsilon|\Phi)$ is the likelihood function, and the multi-dimensional integral $\int_{-\infty}^{+\infty} \cdots \int_{-\infty}^{+\infty} \mathcal{L}(\epsilon|\Phi) f_\Phi(\Phi) d\Phi_1 \cdots d\Phi_l$ is a normalization constant.

The first (updated mean vector $\mu_{\Phi|\epsilon}$) and second (updated covariance matrix $\text{cov}_{\Phi|\epsilon}$) moments of the calibrated model parameters are derived from a second-order approximation of (14) by approximating the natural logarithm of the likelihood function, $g(\Phi) = \ln \mathcal{L}$, with a second-order Taylor series.

https://doi.org/10.1017/S0263574718000024 Published online by Cambridge University Press

The expansion point Φ^*, which maximizes $g(\Phi)$ is then obtained and used to calculate approximations for the updated mean vector $\mu_{\Phi|\epsilon,}$ and the updated covariance matrix $\Sigma_{\Phi|\epsilon}$ using

$$\mu_{\Phi|\epsilon} = \Sigma_{\Phi|\epsilon}\left(\left(\frac{-\partial^2 g}{\partial\Phi_i\partial\Phi_j}\bigg|_{\Phi^*}\right)\Phi^* + \Sigma_{\Phi}^{-1}\mu_{\Phi}\right), \text{ where} \tag{15}$$

$$\Sigma_{\Phi|\epsilon} = \left(\frac{-\partial^2 g}{\partial\Phi_i\partial\Phi_j}\bigg|_{\Phi^*} + \Sigma_{\Phi}^{-1}\right)^{-1}. \tag{16}$$

It should be noted that the updated moments that result from the FSBM method are approximate values. These updated moments are based on prior information and the information contained in the likelihood function. The above formulation assumes that the prior model parameters follow a multivariate normal distribution, and as a result, the approximate distribution of the updated model parameters is also a multivariate normal distribution. The updated mean value obtained using the FSBM is a weighted average of the prior mean value and maximum likelihood point for the data set.[17] Therefore, if more information about a given parameter is provided in the data set (e.g., larger data set of observed measurements), the more this information will be weighted compared to the prior information. The updated covariance matrix (16) calculated by the FSBM provides the updated variance of each parameter and the covariance between each parameter. In addition, correlation coefficients can be calculated between each model parameter to identify related pairs of parameters.

The FSBM was developed to provide a practical Bayesian method for problems with multiple model parameters, large data sets, and various data distributions. As with any First-Order Second-Moment method, the results of the FSBM are considered approximate, especially for cases involving non-linear models and large uncertainties in model parameters.

In this paper, a symbolic programming language, Mathematica®, was used to explicitly compute the first, $\ell'(\tilde{\varphi}^*)$, and second, $\ell''(\tilde{\varphi}^*)$, derivatives of the logarithm of the likelihood function (given in (A3)) evaluated at the expansion point $\tilde{\varphi}^*$. Thus, we have

$$\ell'(\tilde{\varphi}^*) = \frac{\partial\ell}{\partial\tilde{\varphi}_i}\bigg|_{\tilde{\varphi}=\tilde{\varphi}^*}, \text{ and} \tag{17}$$

$$\ell''(\tilde{\varphi}^*) = \frac{\partial^2\ell}{\partial\tilde{\varphi}_i^2}\bigg|_{\tilde{\varphi}=\tilde{\varphi}^*}. \tag{18}$$

Note that $\ell'(\tilde{\varphi}^*)$ is an $l \times 1$ vector while $\ell''(\tilde{\varphi}^*)$ is an $l \times l$ matrix. Here, $\tilde{\varphi}^*$ is the expansion point at which the Taylor series is evaluated and the likelihood is maximized, that is, we have $\tilde{\varphi}^* = \tilde{\varphi}^{MLE}$. Once the derivatives are evaluated, one can estimate the *updated* mean and covariance matrix as indicated in (15) and (16) to arrive at

$$\mu^{pos} = \Sigma^{pos}\cdot\Big(\left(\Sigma^{pri}\right)^{-1}\cdot\mu^{pri} - \ell''(\tilde{\varphi}^*)\cdot\tilde{\varphi}^* - \ell'(\tilde{\varphi}^*)\Big), \text{ where} \tag{19}$$

$$\Sigma^{pos} = \left(\left(\Sigma^{pri}\right)^{-1} - \ell''(\tilde{\varphi}^*)\right)^{-1}, \tag{20}$$

where μ^{pri} and μ^{pos} are respectively the prior and posterior mean vector of model parameters, while Σ^{pos} and Σ^{pos} are respectively the prior and posterior covariance matrices of the model parameters.

4.3. Error bounds

In this section, the value of the novel calibration method is assessed. A main contribution of the paper is embodied in the confidence bounds that the proposed method computes for all measurements. Given the probabilistic nature of the length predictions coupled with the fact that the model parameters are also random variables, there is a need for a systematic approach for combining all sources of uncertainty that affect the predicted length to calculate the expected value and the variance of any length prediction.

https://doi.org/10.1017/S0263574718000024 Published online by Cambridge University Press

For the prior and updated cases, the expected value of any predicted length, $\mathrm{E}(l_{ab})$, and its variance, $\mathrm{var}(l_{ab})$, could be evaluated using a first-order approximation to get

$$\mathrm{E}(l_{ab}) = \mathrm{E}(\mu_{l_{ab}|\tilde{\varphi}}) \tag{21}$$

$$\mathrm{var}(l_{ab}) = \mathrm{E}\left(\sigma_{l_{ab}|\tilde{\varphi}}\right)^2 + \mathrm{var}\left(\sigma_{l_{ab}|\tilde{\varphi}}\right) + \mathrm{var}\left(\mu_{l_{ab}|\tilde{\varphi}}\right), \tag{22}$$

where $\mu_{l_{ab}|\tilde{\varphi}}$ and $\sigma_{l_{ab}|\tilde{\varphi}}$ are the mean value and standard deviation of l_{ab} as indicated in (9) and (10) (both are random variables since they are functions of the uncertain model parameters $\tilde{\varphi}$). It should be noted that (22) indicates that the uncertainty in l_{ab} arises from two sources: random variability that is modeled by the model parameters, $\mathrm{E}\left(\sigma_{l_{ab}|\tilde{\varphi}}\right)^2$ and uncertainty in the model parameters themselves, $\mathrm{var}\left(\sigma_{l_{ab}|\tilde{\varphi}}\right)$ and $\mathrm{var}\left(\mu_{l_{ab}|\tilde{\varphi}}\right)$.

The first and second moments for $\mu_{l_{ab}|\tilde{\varphi}}$ and $\sigma_{l_{ab}|\tilde{\varphi}}$ themselves can be approximated as functions of the first and second moments of the model parameters $\tilde{\varphi}$, using first-order Taylor series expansion such that

$$\mathrm{E}\left(\mu_{l_{ab}|\tilde{\varphi}}\right) = h_\mu\left(\mu_{\tilde{\varphi}}\right) \tag{23}$$

$$\mathrm{var}\left(\mathrm{E}_{l_{ab}|\tilde{\varphi}}\right) = \left\{\left.\frac{\partial h_\mu}{\partial \tilde{\varphi}_i}\right|_{\mu_{\tilde{\varphi}}}\right\}^T \Sigma_{\tilde{\varphi}} \left\{\left.\frac{\partial h_\mu}{\partial \tilde{\varphi}_i}\right|_{\mu_{\tilde{\varphi}}}\right\} \tag{24}$$

$$\mathrm{E}\left(\sigma_{l_{ab}|\tilde{\varphi}}\right) = h_\sigma\left(\mu_{\tilde{\varphi}}\right) \tag{25}$$

$$\mathrm{var}\left(\sigma_{l_{ab}|\tilde{\varphi}}\right) = \left\{\left.\frac{\partial h_\sigma}{\partial \tilde{\varphi}_i}\right|_{\mu_{\tilde{\varphi}}}\right\}^T \Sigma_{\tilde{\varphi}} \left\{\left.\frac{\partial h_\sigma}{\partial \tilde{\varphi}_i}\right|_{\mu_{\tilde{\varphi}}}\right\}, \tag{26}$$

where $\{\frac{\partial h_\mu}{\partial \tilde{\varphi}_i}|_{\mu_{\tilde{\varphi}}}\}$ and $\{\frac{\partial h_\sigma}{\partial \tilde{\varphi}_i}|_{\mu_{\tilde{\varphi}}}\}$ are vectors containing the partial derivatives of $h_\mu(\tilde{\varphi})$ and $h_\sigma(\tilde{\varphi})$, respectively, evaluated at the mean values of the model parameters, and $h_\mu(\tilde{\varphi})$ and $h_\sigma(\tilde{\varphi})$ are the expressions of the probabilistic model of the $\mu_{l_{ab}}$ and $\sigma_{l_{ab}}$, respectively, as reflected in (9) and (10). Hence, using these two equations, the derivatives are computed as follows $\mathcal{J}_{l_{ab}} = \frac{\partial \mu_{l_{ab}}}{\partial \tilde{\varphi}}|_{\mu_{\tilde{\varphi}}}$ and $\mathcal{J}_\sigma = \frac{\partial \sigma_{l_{ab}}}{\partial \lambda}|_{\mu_{\tilde{\varphi}}}$. Accordingly, the variance in the each measurement is comprised of three components,

$$\begin{aligned}
\sigma_{l_{ab}} &= \sqrt{\sigma'^2 + \sigma'' + \sigma'''}, \text{ where} \\
\sigma' &= \sigma_{l_{ab}|\varphi}\big|_{\mu_\varphi}, \text{ using (10)}, \\
\sigma'' &= \mathcal{J}_\sigma^T \cdot \Sigma_{\tilde{\varphi}} \cdot \mathcal{J}_\sigma, \text{ and} \\
\sigma''' &= \mathcal{J}_{l_{ab}}^T \cdot \Sigma_{\tilde{\varphi}} \cdot \mathcal{J}_{l_{ab}}.
\end{aligned} \tag{27}$$

Given the expected value, $\mathrm{E}(l_{ab})$, in (21) and the standard deviation, $\sigma(l_{ab})$, from (27) of the resulting length prediction, l_{ab}, confidence bounds or intervals (e.g., 90% or 95% confidence bounds) can be defined to indicate the expected range of the resulting measurement. This requires an assumption of the probability distribution of $l_{ab,}$ which will be considered in the paper to follow a normal distribution as is the convention.

5. Experimental Setup

In this section, the design of a three degree-of-freedom open-chain robotic arm is introduced. This robotic arm is designed to elaborate the effectiveness of the calibration method discussed in this paper and to validate its utility.

5.1. Mechanical design

The design of the open-chain robotic arm is comprised of three passive revolute joints and four rigid links. At each revolute joint, a rotary encoder is integrated such that it measures the inter-link angle.

https://doi.org/10.1017/S0263574718000024 Published online by Cambridge University Press

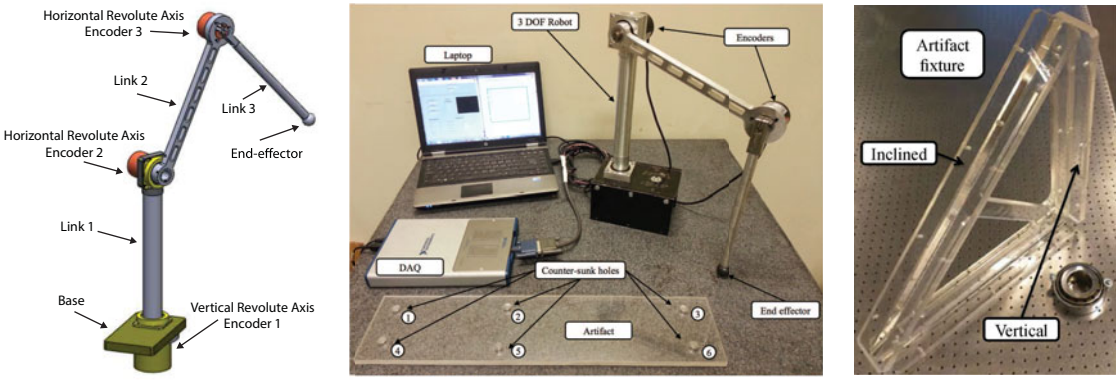

(a) (b) (c)

Fig. 1. (a) A CAD sketch of the three degree-of-freedom manipulator. (b) The actual three degree-of-freedom manipulator, the artifact, the DAQ card, and the computer used to run the calibration software. (c) The artifact fixture used for calibration.

A CAD depiction of the proposed mechanical design is shown in Fig. 1(a). The links are enumerated from 0 to 3 starting at the base and ending at the link on which the end-effector is rigidly attached. Starting from the base, the axes of rotation are vertical, horizontal, and horizontal. The inter-link joints are labeled by encoders 1–3. Note that, at the base, where relatively large forces and torques are expected, the design incorporates a four-point contact bearing, whereas at the other two joints, the integrated encoder bearings were deemed sufficient to carry the loads, and thus no additional bearings were installed.

In this paper, the term manipulator is occasionally used despite the fact that the proposed robotic arm does not have any actuators. Indeed, the robotic arm is completely passive and it requires an operator to articulate its various joints. This robotic platform is similar in structure to measurement robotic platforms used in the industry that are typically referred to as Portable Coordinate Measuring Machines (pCMM),[24] although the adopted design is comprised of a relatively smaller number of joints.

The above manipulator was constructed as shown in Fig. 1(b), which also depicts the artifact with six countersink holes, the data acquisition card, and the laptop that runs the system. The spherical tip of the end-effector is realized by a grade 5 sphere that has a diameter of 12.7 mm. All three joint encoders are Autonics® E50S8-500-3-T-5. Each encoder has 500 lines; that is, each encoder has a maximum resolution of $2\pi/500/4 = 0.00314$ rad. The three encoders are read simultaneously using a high-speed National Instruments® data acquisition card, NI USB-6343 X Series DAQ. Finally, a software was developed in Labview® to acquire data and to perform various simple measurement tasks.

5.2. Kinematic model

Given that the last two joints have parallel axes of rotation, the generalized DH kinematic model is considered robust enough to be used as recommended in refs. [20, 21]. Lumping the level-1 and level-2 parameters into the DH parametrization, five nominal parameters are needed for each joint. The transformation between consecutive coordinate frames can be represented by

$$ {}^{i}_{i-1}T = rot_{\beta_i,y_i}.rot_{\alpha_i,x_i}.trans_{a_i,x_i}.trans_{d_i,z_{i-1}}.rot_{\theta_i,z_{i-1}}, \tag{28} $$

where *rot* and *trans* are homogeneous matrix representations of rotation and translation transformations. Thus, using (3) and the above-mentioned equation one can set $\varphi_i = (\alpha_i, a_i, d_i, \beta_i)$ and $\theta_i = \eta_i + \gamma_i$ for $i = 1, 2, 3$. Here, the typical definitions of the parameters, (α, a, d, β), given in ref. [21], were used.

The kinematics of the manipulator is captured by the nominal generalized D-H parameters in Table I. The link frame assignments using the D-H convention are shown in Fig. 2.

https://doi.org/10.1017/S0263574718000024 Published online by Cambridge University Press

Table I. Nominal generalized DH-parameters of the 3-DOF manipulator (Angles α_i, β_i, and θ_i are in rad and lengths a_i and d_i are in m).

i	α_i	a_i	d_i	$\theta_i = \eta_i + \gamma_i$	β_i
1	1.5708	0.000	0.400	$\eta_1 + 0.0000$	0
2	0.0000	0.295	0.000	$\eta_2 + 2.5133$	0
3	0.0000	0.305	−0.050	$\eta_3 - 0.0126$	0

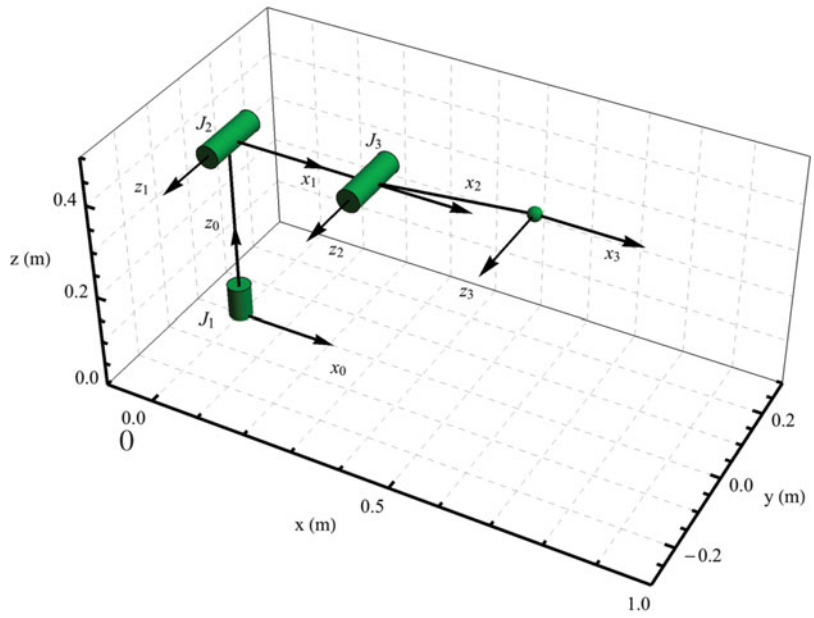

Fig. 2. The kinematic skeleton of the 3-DOF manipulator at its *home* configuration depicting its link's coordinate frames assigned according to the D-H convention and the revolute joints. The cylinders depict the revolute joints while the sphere indicates the end-effector.

Note that the θ column in Table I has numerical values added to the actual encoder angles, η_2 and η_3. These values ($\gamma_1 = 0.000$ rad, $\gamma_2 = 2.5133$ rad, and $\gamma_3 = -0.0126$ rad) indicate offsets in the encoder angles which are due to the level-1 kinematic model and are needed since during assembly, at the home position of the robot as shown in Fig. 2, the encoders typically do not read zero values. As for the first encoder angle, the offset correction is not needed as it just rotates the base frame with respect to an inertial frame. Hence, for getting the nominal values for the DH angle offest parameters, γ_2 and γ_3, the robot was held in its home position and the encoder readings were recorded and added to the fifth column in Table I.

5.3. Parameter set reduction

It is well-known that the generalized DH parametrization is redundant. To make the numerical optimization problem more robust, one should seek a minimal set of kinematic parameters. Referring back to the generalized DH parameter set, it is clear that the parameters a_1, γ_1, d_1, and β_1 can all be ignored. These parameters only affect the configuration of the base frame with respect to an inertial frame. Hence, any volumetric cost function will be invariant with respect to these parameters, and thus should be ignored.

Moreover, since the kinematic model used in this paper neglects the orientation of the end-effector frame, one could possibly neglect more parameters such as α_3 and β_3. Finally, since both d_2 and d_3 are translation along almost parallel joint axes, one of these parameters could be neglected. In this paper, d_2 was chosen to be neglected.

https://doi.org/10.1017/S0263574718000024 Published online by Cambridge University Press

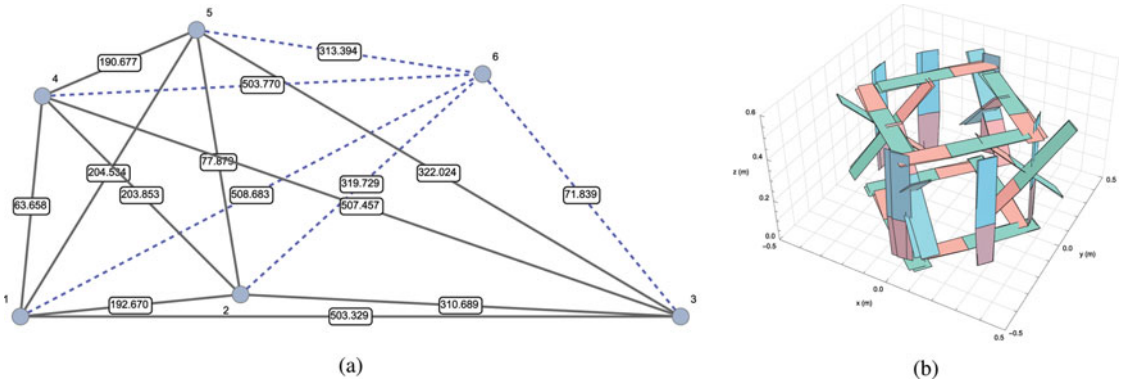

Fig. 3. (a) The locations (not to scale) of the conic holes on the acrylic Plexiglas artifact where the solid lines are used for calibration while dashed lines are used for verification. (b) The various configurations in which the artifact was measured where each rectangle denotes a configuration of the artifact.

Accordingly, only *eight* kinematic parameters, shaded cells in Table I, are needed for the kinematic model, namely

$$\varphi = \begin{pmatrix} a_2 & a_3 & d_3 & \alpha_1 & \alpha_2 & \gamma_2 & \gamma_3 & \beta_2 \end{pmatrix}. \tag{29}$$

5.4. Artifact and fixture

In this paper, the developed calibration algorithms use volumetric data that is based on length measurements between two distinct locations of the end-effector. Accordingly, a special artifact was designed and constructed from a 16 mm thick acrylic Plexiglas® plate to include *six* countersink holes on one face.

The artifact's six countersink holes provide a *stable and repeatable* kinematic seat for the 12.7 mm spherical end-effector. The locations of the countersink holes were measured by a *NIST traceable* pCMM, 2500sc 7-axis Romer Cimcore Infinite 1.0 arm.[24] All 15 possible length measurements between all six holes are depicted in Fig. 3(a) and the lengths range from 63.658 mm to 508.683 mm.

Recall that, for a representative calibration, the manipulator should have measurements in all its reachable and usable space. Accordingly, one needs to position the calibration artifact at many positions and orientations within the manipulator's working space. Additionally, during the artifact measurements, both the artifact and the base of the manipulator should be held rigidly. Otherwise, if a slight motion occurs, the length computed through the forward kinematics and the actual length of the artifact will not be expected to be equivalent. Thus, a triangular fixture shown in Fig. 1(c) was constructed to hold rigidly the artifact which was shown in Fig. 1(b) at various locations and orientations. A single fixture can provide vertical and inclined orientations of the artifact, while two fixtures can be combined – by mounting their inclined plates face-to-face – to allow various levels of horizontal artifact locations.

5.5. Data splitting: calibration versus verification data

To validate the novel calibration method, a complete separation between the measurements used for kinematic calibration and verification is enforced. Additionally, in line with the paramount importance of ensuring uniform measurement distribution per joint and per three-dimensional space, the same conditions are enforced for the calibration and validation data. In other words, the validation measurements should also posses uniform measurement distribution in both the joint space and in the reachable space.

In this paper, the idea of splitting the data for calibration and validation was adopted during the early stages. In fact, this condition shaped the design of the artifact. Recall that the used artifact has six countersink holes located on a rectangular grid on a Plexiglas plate. To separate the measured data, only five holes are used for calibration whereas the sixth hole is used only for validation. Accordingly, for each artifact configuration, a total of 10 length measurements are used for calibration, solid lines in Fig. 3(a), and a total of 5 length measurements are used for validation, dashed lines in Fig. 3(a).

https://doi.org/10.1017/S0263574718000024 Published online by Cambridge University Press

Table II. The various configurations in which the artifact was measured.

Orientation	Vertical level	Second axis	Number
Horizontal	Low	Not flipped	4
Horizontal	Low	Flipped	4
Horizontal	High	Not flipped	4
Horizontal	High	Flipped	4
Vertical	Medium	Not flipped	6
Vertical	Medium	Flipped	6
Inclined	Up	Not flipped	4
Inclined	Up	Flipped	4
Inclined	Down	Not flipped	4
Inclined	Down	Flipped	4
		Total	44

Moreover, all the artifact configurations were used for both calibration and validation. This ensures uniformity of measurements in the reachable three-dimensional space of the manipulators as shown in Fig. 3(b).

5.6. Data collection

For calibration purposes, having measurements uniformly distributed for each joint is of paramount importance. Accordingly, the number of measurements which were performed and the configurations of the artifacts with respect to the manipulator were carefully designed to serve the above-mentioned goal. To ensure a uniform distribution of measurements for the first vertical axis, for each configuration of the artifact, the base of the robot was rotated either four or six times. The last column in Table II indicates the number of rotations for each artifact configuration.

As for articulating the other two joints, Encoders 2 and 3, two measurement methods were employed. The first technique changes the inclination of the artifact from horizontal, to inclined, and finally to vertical. Additionally, horizontal measurements were performed at two vertical levels to improve the uniformity of measurement coverage for Encoders 2 and 3. The first two columns in Table II depict the used artifact configurations. The second technique that was employed to improve the uniformity of measurement was flipping the second joint by almost deg 180. In fact, this capability of flipping is a unique property of our manipulator design. Not only does flipping improve the uniformity of measurement but it also shortens the duration of the calibration routine since flipping the second axis is much faster than moving either the artifact or the base of the robot. In summary, a total of 44 configurations of the artifact were measured as depicted in Table II and all the configurations are shown in Fig. 3(b). Note that each rectangular shape in Fig. 3(b) represents the location and orientation of the artifact with respect to the base of the robot. The corners of the rectangles indicate the locations of the six countersink holes on the artifact.

The uniformity of measurements for Encoder measurements are depicted in Fig. 4. Note that the regions with no measurements indicate configurations in which either the second joint is folded back on the vertical axis or the third joint is folded back on the second link. Both situations are *not* useful reachable spaces for the manipulator.

6. Experimental Validation

In this section, kinematic calibration of the manipulator model parameters is conducted using the conventional regression-based methodology and the novel probabilistic calibration method that is based on the Bayesian inference technique.

6.1. Regression results

The 3-DOF robotic arm investigated in this paper requires the calibration of eight kinematic parameters given in (29). Using the calibration data set of the length measurements (given in Appendix C), and an assumed set of nominal parameter values (given in Table I), one can refer to (6) to compute

https://doi.org/10.1017/S0263574718000024 Published online by Cambridge University Press

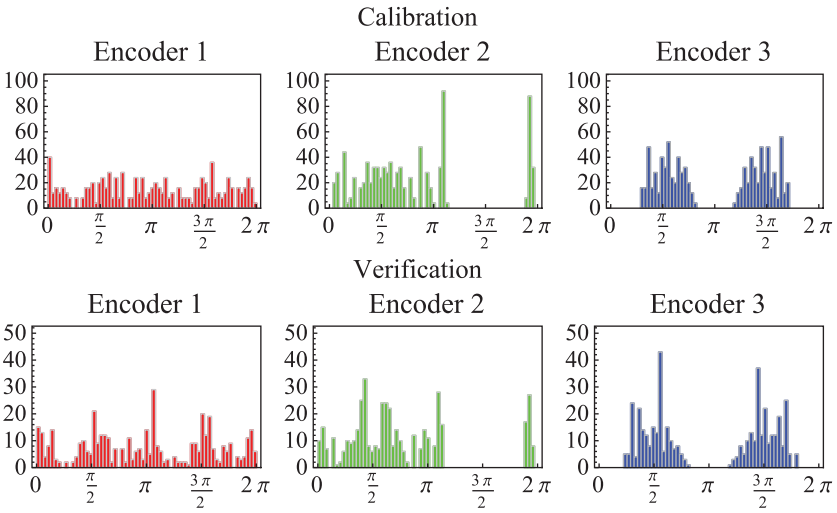

Fig. 4. The histogram depicting the coverage of the measurements for each encoder for both the calibration and verification data.

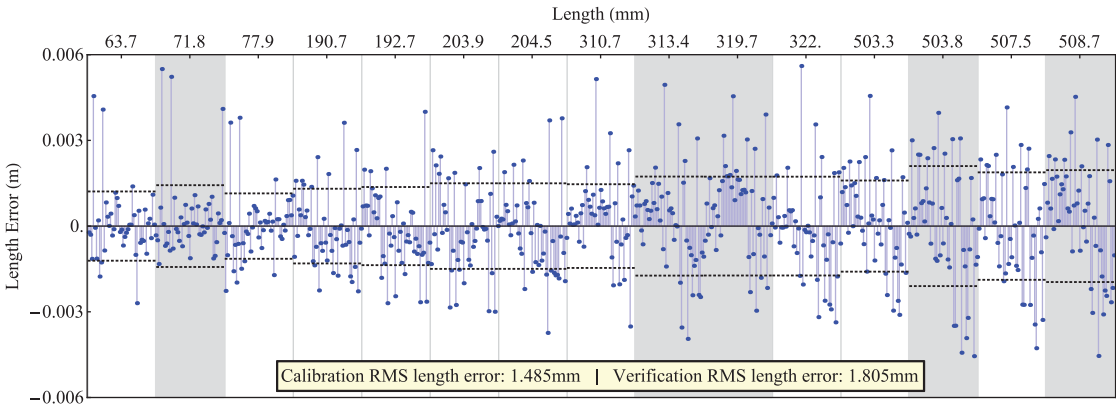

Fig. 5. The individual length measurement errors for the calibration (not shaded) and verification (shaded).

the total RMS error that is a function of the deviation of the kinematic model parameters such that $ERR(\tilde{\varphi}) = ERR(\tilde{a}_2, \tilde{a}_3, \tilde{d}_3, \tilde{\alpha}_1, \tilde{\alpha}_2, \tilde{\gamma}_2, \tilde{\gamma}_3, \tilde{\beta}_2)$.

The function, $ERR(\tilde{\varphi})$, is *minimized* using a non-linear solver to arrive at an optimal set of calibration parameters depicted in Table III. The shaded cells in the table indicate the parameters which were optimized, while all other parameters were held constant during the optimization.

The resulting measured length errors for the calibration data are depicted in Fig. 5. Recall that the artifact was measured 44 times and for each artifact configuration, 10 calibration lengths and 5 verification lengths were acquired. Hence, $440 = (44 \times 10)$ calibration length errors were computed as indicated in the non-shaded regions in Fig. 5, whereas $220 = (44 \times 5)$ verification length errors were computed and presented as the shaded regions in Fig. 5.

In the presentation of the individual length measurement errors in Fig. 5, the length errors were sorted by length. Additionally, for each length, the dashed lines indicate the RMS of all the length errors for that particular length. The bounds set by the dashed lines give a good *indication* of the accuracy of the manipulator for that particular length. It is worth noting that this accuracy bound gets larger for larger measured lengths.

Results in Fig. 5 indicate that the RMS errors for the calibration and verification data are 1.49 mm and 1.81 mm, respectively (see Table IV). For comparison, the corresponding RMS errors for the case where the nominal parameters are used in the kinematic model instead of the calibrated model

https://doi.org/10.1017/S0263574718000024 Published online by Cambridge University Press

Table III. The regression revised DH-parameters of the real 3-DOF manipulator (Angles α_i, β_i, and θ_i are in rad and lengths a_i and d_i are in m).

i	α_i	a_i	d_i	$\theta_i = \eta_i + \gamma_i$	β_i
1	1.5793	0.0000	0.4000	η_1	0.0000
2	0.0091	0.2921	0.0000	$\eta_2 + 2.481$	−0.0221
3	0.0000	0.3089	−0.0520	$\eta_3 - 0.0321$	0.0000

Table IV. The calibration and verification root mean square error for the nominal and calibrated kinematic parameters.

RMS error mm Err($\bar{\varphi}$)	Nominal parameters $\bar{\varphi} = \varphi$	Calibrated parameters $\bar{\varphi} = \varphi + \tilde{\varphi}$
Calibration data	8.47	1.49
Verification data	10.4	1.81

parameters are very high, reaching RMS values of 8.47 mm for the calibration date and 10.4 mm for the verification data (see also Table IV). These results indicate the importance of the calibration procedure in determining the optimal parameters for any given robotic arm.

Finally, it is very important to treat the overall RMS error of the verification data as an *estimate* of the accuracy of the manipulator. In fact, many CMM manufacturers use similar methods to report the accuracy of their measuring products.[2,29] Such certification methods do not measure the uncertainty of the machine nor do they allow for the direct computation of the uncertainty in any future measurement. The proposed probabilistic calibration method will be presented in the following section.

6.2. Updating model parameters using Bayesian inference

In this section, the proposed calibration method is applied to the three degree-of-freedom robotic platform. The section is divided into three major parts dealing with prior statistics, posterior statistics, and error bounds.

6.2.1. Prior mean and covariance. In the probabilistic Bayesian approach that was presented in Section 4, the length measurement is assumed to be a random variable that is characterized by a mean and standard deviation which were defined by (9) and (10), respectively. The mean of the length measurement in (9) is a function of the eight kinematic model parameters, which in the framework of this paper, are defined as the deviations of the kinematic parameters from their nominal values. A ninth parameter that completes the probabilistic model is the parameter λ, which defines the standard deviation of the length measurement as indicated in Eq. (10). As a result, the parameters that need to be updated based on the collected set of measurements are

$$\tilde{\varphi} = \begin{pmatrix} \tilde{a}_2 & \tilde{a}_3 & \tilde{d}_3 & \tilde{\alpha}_1 & \tilde{\alpha}_2 & \tilde{\gamma}_2 & \tilde{\gamma}_3 & \tilde{\beta}_2 & \tilde{\lambda} \end{pmatrix}. \tag{30}$$

The first step in the updating process involves defining the prior statistics of the model parameters representing length, namely $\tilde{a}_2$, $\tilde{a}_3$, and $\tilde{d}_3$, angles, namely $\tilde{\alpha}_1$, $\tilde{\alpha}_2$, $\tilde{\gamma}_2$, $\tilde{\gamma}_3$, and $\tilde{\beta}_2$, the length measurement uncertainty parameter $\tilde{\lambda}$.

The prior mean values of the kinematic model parameters can be estimated to be the nominal values that are readily available from manufacturer's data. This can be accomplished by utilizing sub-assembly measurements or by controlling assembly procedures. Accordingly, once the nominal values are estimated (see Table I), the prior mean values for the deviations of the kinematic parameters can be estimated to be zero.

As for the measurement uncertainty, $\tilde{\lambda}$, which defines the standard deviation of the length measurements, one can estimate its prior mean value from estimates of the anticipated volumetric

https://doi.org/10.1017/S0263574718000024 Published online by Cambridge University Press

error of the robotic arm. A quick simulation of the arm's forward kinematics using the nominal values of the kinematic parameters and the encoder resolution can be used to estimate the error in the position of the end-effector. For the 3-DOF example presented in this paper, the expected standard deviation of the length measurements is estimated to be in the order of 4 mm. Accordingly, the prior mean value for the parameter $\tilde{\lambda} = \log 0.004 = -5.521$.

$$\left(\mu^{pri}, \sigma^{pri}\right) = \begin{pmatrix} 0.0 & 0.00100 \\ 0.0 & 0.00100 \\ 0.0 & 0.00100 \\ 0.0 & 0.00314 \\ 0.0 & 0.00314 \\ 0.0 & 0.00314 \\ 0.0 & 0.00314 \\ 0.0 & 0.00314 \\ -5.521 & 0.19711 \end{pmatrix}. \tag{31}$$

Regarding the prior standard deviations of the model parameters, it is estimated that the standard deviations of the length and angle sets can be taken as $\epsilon_{len} = 1$ mm and $\epsilon_{ang} = \frac{u_0}{2} = 0.00314$ rad, respectively. Here, 1 mm is the typical uncertainty due to manufacturing tolerances and assembly variations whereas the angle uncertainty is equated to half the used encoder resolution u_0. Note that, for other manipulators, the prior standard deviations for kinematic parameters pertaining to lengths and angles can be estimated using stacked tolerance analysis.[49] Additionally, a manufacturer can draw on information from the quality control department of inspections of parts and sub-assemblies to estimate such prior information.

The prior standard deviation in the uncertainty measurement was estimated by assuming that the range of $\sigma_{l_{ab}}$ could be defined by the mean value (which is equal to 4.0 mm) ± 1.5 mm, leading to a range of 2.5 mm–5.5 mm. Assuming that this range covers plus and minus two standard deviations about the estimated mean value of 4 mm, the prior standard deviation for the uncertainty measurement could be estimated as

$$\begin{aligned} \sigma_{\tilde{\lambda}}^{pri} &= \frac{\log(0.004 + 0.0015) - \log(0.004 + 0.0015)}{4} \\ &= 0.19711. \end{aligned}$$

The resulting prior means and standard deviations of the nine random model parameters are given in (31). In the initial analysis, it will be assumed that there is no statistical correlation between the different model parameters, that is, $\rho^{pri} = \mathbb{I}^{9\times 9}$. This results in a prior diagonal covariance matrix for the model parameters such that, $cov_{ii}^{pri} = \left(\sigma_i^{pri}\right)^2$.

6.2.2. Posterior mean and covariance. The set of length measurements which were designated for calibration were used to update the prior statistics of the nine model parameters shown in (31). The FSBM as formulated in ref. [17] was used for that purpose. The resulting updated/posterior mean vector and covariance matrix of the model parameters are solved for and used to calculate the vector of the standard deviations and the correlation matrix of the model parameters using

$$\rho_{ij}^{pos} = \frac{cov_{ij}^{pos}}{cov_{ii}^{pos} cov_{jj}^{pos}}, \text{ and} \tag{32}$$

$$\sigma_i^{pos} = \sqrt{cov_{ii}^{pos}}. \tag{33}$$

https://doi.org/10.1017/S0263574718000024 Published online by Cambridge University Press

Accordingly, the posterior mean and standard deviations of the model parameters are computed to get

$$\left(\mu^{pos}, \sigma^{pos}\right) = \begin{pmatrix} -0.002602 & 0.000193 \\ 0.003528 & 0.000264 \\ -0.003382 & 0.000687 \\ 0.006169 & 0.001221 \\ 0.005237 & 0.0018 \\ -0.030443 & 0.000818 \\ -0.02013 & 0.000682 \\ -0.015833 & 0.00181 \\ -6.12994 & 0.046337 \end{pmatrix}. \tag{34}$$

A comparison between the prior and updated mean values of the deviations of the kinematic model parameters indicates that the posterior mean deviations in the length parameters are in the order of ± 3.5 mm from the prior nominal values. For the angle parameters, the posterior mean deviations range from about -0.03 rad to 0.005 rad about the prior nominal values. With regard to the parameter λ which defines the standard deviation in the length measurements, the posterior results indicate that mean value of λ decreased from -5.52 (for the prior case) to a value of -6.13 (after updating). These results indicate that the mean value of the standard deviation of the length measurements, which was estimated in the prior model to be in the order 4 mm, was reduced almost in half to a value of 2.18 mm after calibration. It should be noted that the standard deviation of the length measurements is expected to play a significant role in determining the confidence bounds of any length measurement that is predicted using the robotic arm under study.

On the other hand, a comparison between the prior and posterior standard deviations of the model parameters leads to several observations. For the length parameters, the estimates of the standard deviations were reduced significantly following the updating process. The reduction was in the order of 4–5 folds for parameters a_2 and a_3 (reduction from 1 mm to 0.2 mm and 0.26 mm, respectively) and 1.5 folds for d_3 (reduction from 1 mm to 0.68 mm). Similar reductions in the standard deviations of the angle parameters were observed with 1.7–4.6 folds reduction in the standard deviation. These results are significant since they indicate that the Bayesian updating process not only leads to more realistic estimates of the mean model parameters, but it also leads to reductions in the level of uncertainty in the calibrated model parameters in comparison to the prior values. This will, in turn, lead to narrower confidence bounds for any length prediction using the calibrated robotic arm. As to the parameter λ, the updated model parameters indicate that the uncertainty in λ also decreased as reflected in the standard deviation which was found to decrease from 0.197 to 0.046. These reductions reflect more confidence in the updated standard deviation of the length measurements $\sigma_{l_{ab}}$ which can be shown to fall within the narrow range of 1.98 mm–2.38 mm for the posterior case, compared to the wide range of 2.5 mm–5.5 mm in the prior case. Since the standard deviation of λ is a contributor to the total uncertainty in any predicted length measurement (see Eq. (22)), it can be concluded that the updating process results in a set of posterior model parameters that would provide narrower confidence bounds and improved reliability compared to the prior cases.

In addition to the posterior mean and standard deviations, the Bayesian updating process allows for the quantification of any statistical correlation that may exist among the different pairs of model parameters. These correlations are reflected in the non-diagonal entries of the covariance matrices of the model parameters and can be quantified through Eq. (32). For comparison, a plot showing the prior and posterior correlation matrices is depicted in Fig. 6 where it is clear that although the model parameters were assumed to be statistically independent in the prior case, the calibration data resulted in updated correlation coefficients that are non-zero between several model parameters. As an example, the posterior results indicate that negative correlation exists between γ_1 and γ_2 as reflected in the correlation coefficient of -0.559, which is due to the fact that the second and third joint axes are almost parallel. Another even stronger negative correlation is between d_2 and β_1. Referring to Fig. 2, this also is understandable since the axes of joints second and third are almost parallel, and the intersection of their common perpendicular with the first axis which defines d_2 could vary wildly as β_1 changes. This result makes sense since both angles are rotations about almost parallel horizontal axes. Moreover, the positive sense of rotations are both clockwise hence the negative correlation.

https://doi.org/10.1017/S0263574718000024 Published online by Cambridge University Press

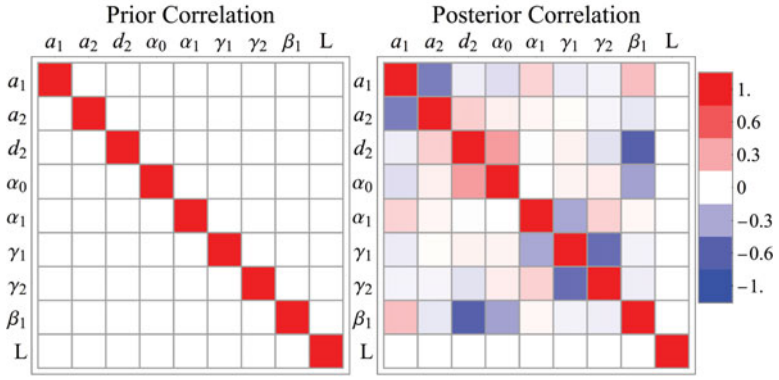

Fig. 6. Correlation matrices of the prior and posterior covariance matrices, showing strong positive correlation between α_0 and d_2 and strong negative correlation between β_1 and d_2 in the posterior model.

Another thing to note is the expected and realistically small to negligible correlation coefficients between the length parameters and the angle parameters. Finally, note the "zero" correlation between the measurement error parameter λ and all other parameters. This is expected given that λ is not a kinematic parameter but rather a length measurement parameter.

6.2.3. Length confidence bounds for prior and posterior models. The added value of the fully probabilistic length prediction model of the robotic platform lies in the ability to predict lengths in the form of confidence bound intervals. This could be achieved for both the prior and updated model parameters. Consider the measurements conducted for the shortest artifact length ($L_{14} = 63.658$) between conic holes one and four in Fig. 3(a). Note that 44 length measurements with different configurations were conducted for each artifact length as indicated in Section 5.6. For each of the 44 measurements, a mean predicted length $E(l_{14})$ and an overall standard deviation $\sigma(l_{14})$ can be obtained using Eqs. (23) and (27), respectively. $E(l_{14})$ and $\sigma(l_{14})$ will differ depending on whether the prior or updated model parameters are used. The difference between the mean predicted length $E(l_{14})$ and the actual artifact length ($l_{14} = 63.658$ mm) is an indication of the mean length measurement error. This mean length error is shown in Fig. 7(a) for the 44 measurements corresponding to L_{14} using the prior model parameters of the robotic arm. It is interesting to observe that even for the same artifact length, the mean errors from the different measurements differ depending on the configuration of the artifact and the robotic platform. The same applies to the predicted standard deviation of each length measurement $\sigma_{l_{14}}$, which could be used to construct confidence bounds (or error bounds) for the length measurement predicted by the robotic platform. For illustration, confidence bounds corresponding to $\pm 2\sigma_{l_{14}}$ are drawn in Fig. 7(a) for each measurement of l_{14} to reflect the uncertainty in the length predictions. To add clarity to the presentation of the data, the 44 measurements were sorted such that the measurements having the smallest error bounds are to the left and those with the largest bounds are to the right (see Fig. 7(b)). It should be also noted that for a typical Gaussian distribution, confidence intervals that are bounded by $\pm 2\sigma$ reflect 95% confidence in the predicted value.

The results in Fig. 7 indicate that not all the predicted length errors for L_{14} in the prior model lie within the 95% confidence bound interval. In fact, only 75% of the errors lie within the designated bounds although the error bounds could be considered to be relatively large (around $\pm$ 8.5 mm). Note that the dashed lines in Fig. 7 indicate predicted length error outside the scale of the plot. This result is important since it indicates that the parameters that were assumed in the prior model may not be accurate leading to wide error bounds that do not yield the desired level of confidence. The role of the Bayesian updating methodology that was adopted in this paper is to use the data collected to update the model parameters with the objective of getting narrower error bounds with a consistent target level of confidence. This is clearly indicated in Fig. 7(c) and (d) which show the 44 mean length errors and 95% confidence bounds for L_{14} using the updated model parameters. Results indicate that the 95% confidence bounds are much narrower (around $\pm$ 4 mm) owing to the improved mean estimates of the updated model parameters and their reduced uncertainty. More importantly, all of the actual artifact lengths fall within the 95% error bounds indicating a high level of reliability in reporting

https://doi.org/10.1017/S0263574718000024 Published online by Cambridge University Press

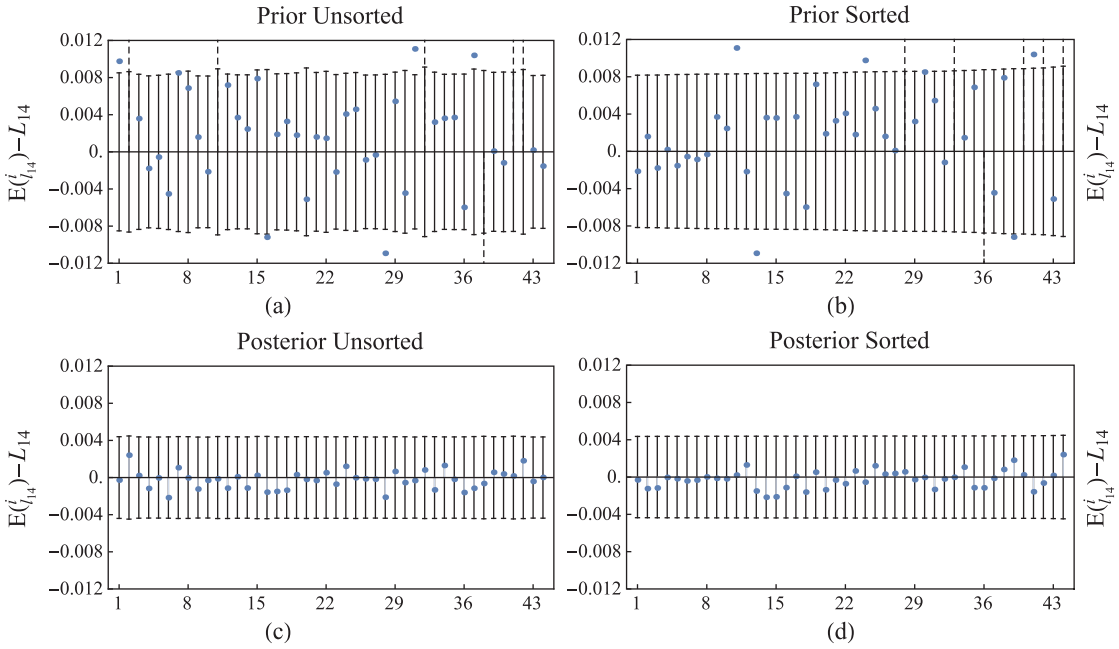

Fig. 7. Prior and posterior mean length errors and associated 95% confidence bounds for artifact length L_{14}.

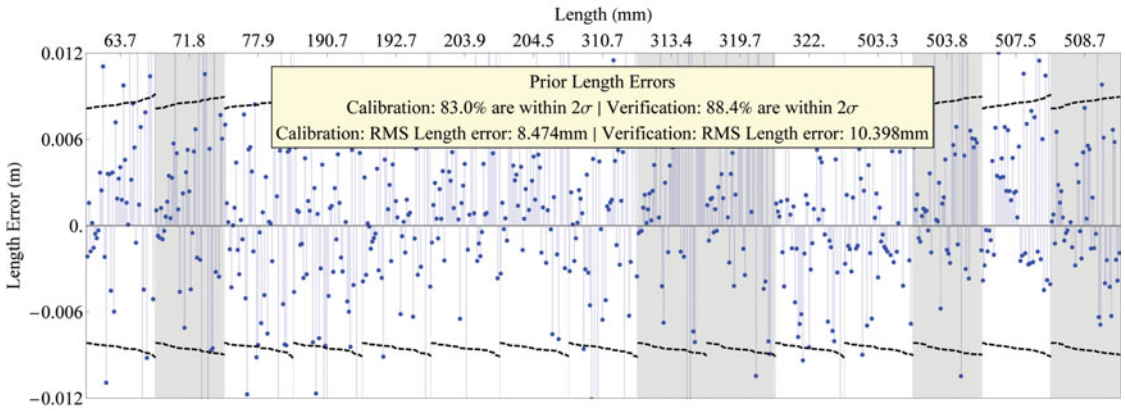

Fig. 8. Prior mean length errors: Calibration lengths are not shaded, verification lengths are shaded. Dashed lines indicated the prior 95% error bounds.

confidence intervals in the updated model. Similar to the prior case, Fig. 7(c) and (d) present the same information; however, in Fig. 7(d) the data is sorted by the magnitude of the 95% confidence bounds.

The data presented in Fig. 7 represents only one artifact length (L_{14}) out of 10 "calibration" lengths that were used in the calibration/updating exercise. The data collected in this study also includes an additional five sets of length measurements that were designated as "verification". The intent was to use this data set to verify the performance of the calibrated/updated model with an independent set of measurements. Both calibration and verification data for all artifact lengths were combined in Fig. 8 (prior model) and Fig. 9 (updated model) to reflect the mean errors of the different length predictions and their associated 95% confidence bounds. The data is essentially identical in format to that analyzed in Fig. 7(b) and (d) for artifact length (L_{14}), except that "calibration" cases are presented in non-shaded columns while "verification" cases are presented in shaded columns.

Results shown in Fig. 8 indicate that for the "calibration" data set, only 83% of the actual measurements fall within the 95% confidence bounds for the cases involving the prior model parameters. This percentage increases to 88.4% for the "verification" data set. Additionally, the RMS of the calibration and verification mean length errors were computed and found to be equal to

https://doi.org/10.1017/S0263574718000024 Published online by Cambridge University Press

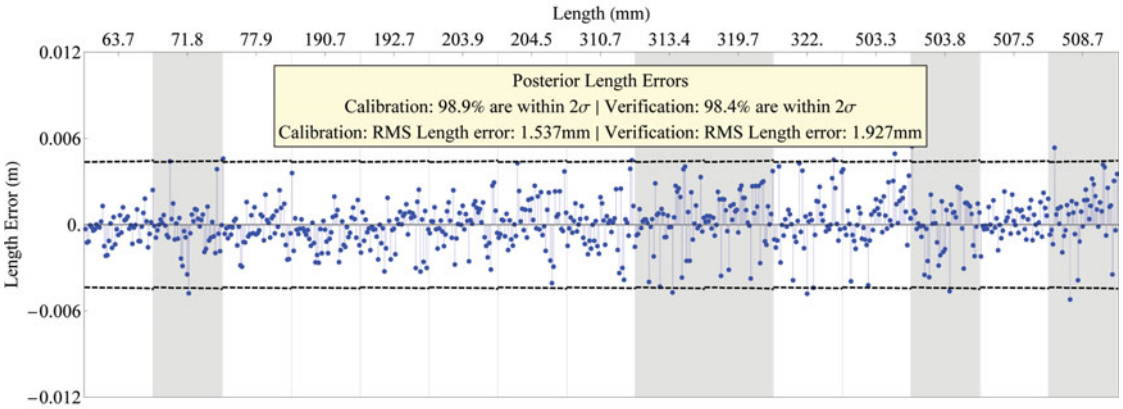

Fig. 9. Posterior mean length errors: Calibration lengths are not shaded, verification lengths are shaded. Dashed lines indicated the prior 95% error bounds.

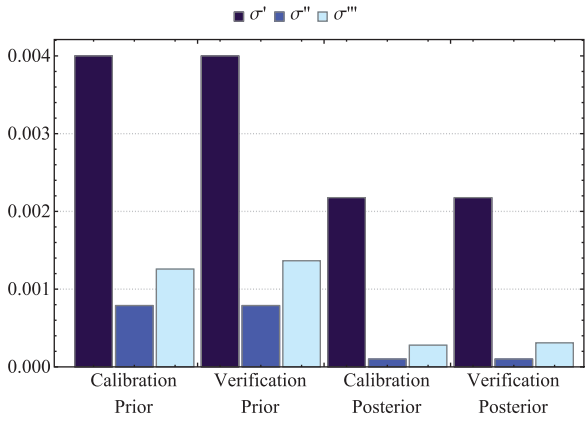

Fig. 10. The various components of uncertainty for both the prior and posterior model.

8.474 mm and 10.398 mm, respectively. The above RMS mean length errors are considered to be large indicating that the prior model parameters do not provide an efficient model for the robotic arm length predictions. On the other hand, results pertaining to the updated posterior model parameters in Fig. 9 indicate a clear improvement in accuracy and reliability of the length predictions, with a substantial observed reduction in the 95% confidence error bounds. For the updated case, the percentage of "calibration" length errors that are within the $\pm 2\sigma$ increased to 98.9% whereas the percentage of "verification" length errors that are within the $\pm 2\sigma$ increased to 98.4%. This improvement in length errors that are within the denoted bounds was realized despite the fact that the error bounds themselves were reduced dramatically. Moreover, an investigation of the RMS of the calibration and verification mean length errors for the posterior cases indicates that the RMS of the "calibration" length errors was reduced to 1.537 mm (compared to 8.474 mm for the prior case) while the RMS of the "verification" length errors was reduced to 1.927 mm (compared to 10.398 mm).

It is worth noting that despite the significant reduction in the RMS for the posterior case, the RMS values (1.537 mm and 1.927 mm) remain to be slightly larger than the RMS observed in the regression analysis (1.49 mm and 1.81 mm). This is expected given the nature of the Bayesian updating formulation which considers the weights of both the prior model parameters and the collected data in its formulation.

It should be reiterated that the 95% confidence bounds that are shown in Figs. 7–9 are defined based on the total standard deviation (prior or posterior) of the predicted artifact length. This standard deviation is comprised of three components as indicated in (27). The contribution of these components to the total uncertainty is illustrated in Fig. 10 for the calibration and verification data and for the prior and posterior models. Results in Fig. 10 indicate that the main contributor to the total uncertainty in the predicted artifact length is σ' which constitutes more than 2/3 of the total uncertainty in the

https://doi.org/10.1017/S0263574718000024 Published online by Cambridge University Press

Table V. The effect of prior correlation assumption on the updated calibration results. The units for all errors are in mm while the last row is percentages. Shaded cells indicate values that are independent on the prior correlation and thus remain fixed.

	$\rho = 0.0$				$\rho = 0.2$				$\rho = 0.5$			
	Calibration		Verification		Calibration		Verification		Calibration		Verification	
	Pri	Pos	Pri	Pos	Pri	Pos	Pri	Pos	Pri	Pos	Pri	Pos
Err ($\tilde{\varphi}$)	8.474	1.537	10.398	1.927	8.474	1.564	10.398	1.960	8.474	1.654	10.398	2.078
σ'	4.000	2.177	4.000	2.177	4.000	2.177	4.000	2.177	4.000	2.177	4.000	2.177
σ''	0.789	0.101	0.789	0.101	0.789	0.101	0.789	0.101	0.789	0.101	0.789	0.101
σ'''	1.370	0.299	1.461	0.333	1.433	0.296	1.545	0.329	1.530	0.286	1.671	0.318
% errors within C.I.	83.0	98.9	88.4	98.4	83.0	98.9	88.6	98.4	83.6	97.0	88.6	97.3

prior model and more than 85% of the total uncertainty in the updated model. The second major contributor is σ''' which reflects the uncertainty in the kinematic model parameters of the robotic arm. The contribution of σ''' is around 25% in the prior model decreasing to less than 15% in the posterior model. Note that σ''' varies from one measurement to the other whereas the other two components of the total uncertainty are constant for all the measurements. The values of σ''' that are reported in Fig. 10 are *average* values for all measurements. Finally, the results on Fig. 10 show clearly how the different source of uncertainty decrease substantially for the posterior case in comparison to the prior case, leading to an overall reduced total uncertainty in the posterior model.

7. Discussion

Results presented in Section 6 indicate clearly the added value behind utilizing the Bayesian method in a fully probabilistic framework that is aimed at calibrating the parameters of the robotic platform and quantifying the uncertainty associated with the resulting length predictions. Given this added value, questions could be raised regarding the sensitivity of the results to the assumptions made with regard to the statistical properties of the prior model parameters. This section aims at answering these questions by examining the sensitivity of the Bayesian results to the prior model assumptions pertaining to (1) the assumed prior correlation between the different model parameters, and (2) the assumed prior mean value for the parameter λ which defines the prior mean value of the standard deviation of L_{ab}.

The sensitivity of the posterior results to the assumed prior correlation between model parameters was studied by considering three correlation cases. The first case is the base case where all parameters are assumed to be statistically independent (adopted in the previous section). In addition to the base case, two cases were studied whereby all "length" and "angle" parameters of the robotic arm were assumed to be correlated positively. Several correlation coefficients were assumed in the sensitivity analysis including $\rho = 0$ (no correlation), $\rho = 0.2$ (weak positive correlation), and $\rho = 0.5$ (stronger positive correlation). Results of the Bayesian updating exercise are presented in Table V and indicate that the assumption of the prior correlation between parameters has a negligible effect on the results. With regard to the mean length error of the posterior length predictions, results in Table V indicate that the RMS of the errors of the "verification" cases slightly increases from 1.927 mm (no correlation $\rho = 0$) to 2.078 mm (for the case with correlation $\rho = 0.5$). On the other hand, an associated marginal decrease in σ''' is observed with values decreasing from 0.333 mm for the no correlation case to 0.318 mm for the case with a correlation coefficient of $\rho = 0.5$. As expected, these negligible effects of the correlation assumption in the prior model did not have any major influence on the confidence bounds intervals of the updated model. For illustration, the percentage of predictions that fall within the 95% confidence bounds for the "verification" data decreased slightly from 98.4% to 97.3%.

Similarly, the sensitivity of the posterior results to the assumed prior mean value for the parameter λ was studied by considering three cases. The first case is the base case where the prior mean of λ was chosen to yield a prior mean standard deviation of L_{ab} equal to 4 mm. This assumption was adopted

https://doi.org/10.1017/S0263574718000024 Published online by Cambridge University Press

Table VI. The effect of mean value for the parameter λ on the updated calibration results. The units for all errors are in mm while the last row is percentages. Shaded cells indicate values that are independent on the prior correlation and thus remain fixed.

	$e^{\lambda} = 0.002$ mm				$e^{\lambda} = 0.004$ mm				$e^{\lambda} = 0.006$ mm			
	Calibration		Verification		Calibration		Verification		Calibration		Verification	
	Pri	Pos	Pri	Pos	Pri	Pos	Pri	Pos	Pri	Pos	Pri	Pos
Err ($\tilde{\varphi}$)	8.474	1.537	10.398	1.927	8.474	1.537	10.398	1.927	8.474	1.537	10.398	1.927
σ'	2.000	2.100	2.000	2.100	4.000	2.177	4.000	2.177	6.000	2.388	6.000	2.388
σ''	0.973	0.100	0.973	0.100	0.789	0.101	0.789	0.101	0.766	0.107	0.766	0.107
σ'''	1.370	0.299	1.461	0.333	1.370	0.299	1.461	0.333	1.370	0.299	1.461	0.333
% errors within C.I.	63.6	98.2	77.3	98.2	83.0	98.9	88.6	98.4	89.8	99.8	91.4	99.3

in all the analyses conducted in this study so far. In the sensitivity analysis, two other cases whereby the prior mean standard deviation of L_{ab} was taken as 2 mm and 6 mm were adopted. These cases represent realistic lower and upper bounds of the prior mean estimate of the standard deviation of the robotic platform. Results of the Bayesian updating exercise with different prior mean estimates of the standard deviation of L_{ab} are presented in Table VI and indicate a negligible effect on the results. For example, the RMS of the posterior mean length errors of the "verification" cases remained fixed at a value of about 1.927 mm, irrespective of the prior mean standard deviation of L_{ab}. On the other hand, the posterior values of σ' and σ'' (which are directly affected by the mean standard deviation of L_{ab}) exhibited slight decreases (see Table VI) for the case where the prior mean standard deviation of L_{ab} was reduced to 2 mm and slight increases for the case where the prior values were increased to 6 mm. In fact, the posterior value of σ' in the verification cases increased from 2.100 mm to 2.388 mm when the prior estimate of the mean standard deviation of L_{ab} was increased from 2 mm to 6 mm. The corresponding increase in σ'' was from 0.100 mm to 0.107 mm. The effect of the changes on the confidence bounds intervals of the updated models was negligible. For illustration, the percentage of predictions that fall within the 95% confidence bounds for the "verification" data increased slightly from 98.2% to 99.3%.

The above analyses indicate that the results of the updating process are relatively insensitive to the assumed prior model parameters. This adds robustness to the results of the updating process and increases confidence in the posterior model parameters.

8. Conclusion

In this paper, a novel probabilistic kinematic calibration method for serial robotic arms was presented. In the proposed method, the parameters of the kinematic model of the robotic platform are considered to be random variables that could be updated within a Bayesian framework using a new set of measurements. As opposed to typical regression based calibration methods, the proposed technique incorporates prior information about the kinematic model parameters and utilizes measured data to update the statistical characteristics of the model parameters. The fully probabilistic nature of the updated kinematic model allows for allocating realistic and reliable confidence bounds to the individual length predictions that are associated with the calibrated robotic arm. This constitutes an added value in comparison to other traditional calibration methods that are based on deterministic methodologies.

To test the robustness of the proposed probabilistic calibration framework, a three degree-of-freedom robotic arm was designed and constructed and extensive measurements were collected. The real measurements indicated that the proposed probabilistic calibration approach is effective at updating the prior model parameters and yields mean errors that are comparable to those obtained using regression-based methods. The main advantage of the method is in its ability to yield reliable 95% confidence bound error intervals. The robustness of the method was proven through sensitivity studies whereby the results of the updating process were shown to be relatively insensitive to

https://doi.org/10.1017/S0263574718000024 Published online by Cambridge University Press

some of the assumptions that need to be made in assigning prior estimates of some of the model parameters.

Finally, it is worth noting that the approach that is proposed in this paper could be used in future studies to identify sweet spots or manipulator configurations where tight error bounds exit.

References

1. S. Aoyagi, A. Kohama, Y. Nakata, Y. Hayano and M. Suzuki, "Improvement of Robot Accuracy by Calibrating Kinematic Model Using a Laser Tracking System-Compensation of Non-Geometric Errors Using Neural Networks and Selection of Optimal Measuring Points Using Genetic Algorithm," *Proceedings of the IEEE/RSJ International Conference on Intelligent Robots and Systems (IROS)* (2010) pp. 5660–5665.
2. ASME B89, "ASME B89.4.22-2004, methods for performance evaluation of articulated arm coordinate measuring machines," Technical report, ASME (2004).
3. D. J. Bennett, D. Geiger and J. M. Hollerbach, "Autonomous robot calibration for hand-eye coordination," *Int. J. Robot. Res.* **10**(5), 550–559 (1991).
4. J. H. Borm and C. H. Meng, "Determination of optimal measurement configurations for robot calibration based on observability measure," *Int. J. Robot. Res.* **10**(1), 51–63 (1991).
5. S. Brooks, A. Gelman, G. Jones and X. L. Meng, *Handbook of Markov Chain Monte Carlo*. Chapman & Hall/CRC Handbooks of Modern Statistical Methods. (Boca Raton, FL, U.S.A., CRC Press/Taylor & Francis, 2011).
6. J. Chen and L. M. Chao, "Positioning error analysis for robot manipulators with all rotary joints," *IEEE J. Robot. Autom.* **3**(6), 539–545 (1987).
7. J. T. Christian and G. B. Baecher, "Point-estimate method as numerical quadrature," *J. Geotech. Geoenvironmental Eng.* **125**(9), 779–786 (1999).
8. D. Daney, Y. Papegay and B. Madeline, "Choosing measurement poses for robot calibration with the local convergence method and tabu search," *Int. J. Robot. Res.* **24**(6), 501–518 (2005).
9. J. Denavit and R. S. Hartenberg, "A kinematic notation for lower-pair mechanisms based on matrices," *Trans. ASME J. Appl. Mech.* **22**, 215–221 (1955).
10. M. R. Driels and U. S. Pathre, "Vision-based automatic theodolite for robot calibration," *IEEE Trans. Robot. Autom.* **7**(3), 351–360 (1991).
11. M. R. Driels, L. W. Swayze and L. S. Potter, "Full-pose calibration of a robot manipulator using a coordinate-measuring machine," *Int. J. Adv. Manuf. Technol.* **8**(1), 34–41 (1993).
12. C. Dumas, S. Caro, M. Cherif, S. Garnier and B. Furet, "A Methodology for Joint Stiffness Identification of Serial Robots," *Proceedings of the IEEE/RSJ International Conference on Intelligent Robots and Systems (IROS)* (2010) pp. 464–469.
13. C. A. Edwards and R. L. Galloway, "A single-point calibration technique for a six degree-of-freedom articulated arm," *Int. J. Robot. Res.* **13**(3), 189–198 (1994).
14. L. J. Everett, "Forward calibration of closed-loop jointed manipulators," **8**(4), 85–91 (1989).
15. C. S. Gatla, R. Lumia, J. Wood and G. Starr, "An automated method to calibrate industrial robots using a virtual closed kinematic chain," *IEEE Trans. Robot.* **23**(6), 1105–1116 (2007).
16. A. Gelman, J. B. Carlin, H. S. Stern and D. B. Rubin, "*Bayesian Data Analysis*, volume 2 (Chapman & Hall/CRC Boca Raton, FL, USA, 2014).
17. R. Gilbert, "First-order, second-moment Bayesian method for data analysis in decision making," Technical report, Department of Civil Engineering, The University of Texas at Austin (1999).
18. H. Zhuang, "A note on the use of identification Jacobians for robot calibration," *Int. J. Robot. Res.* **14**(1), 87–89 (1995).
19. R. S. Hartenberg and J. Denavit, *Kinematic Synthesis of Linkages*. McGraw-Hill series in mechanical engineering. (New York, NY, U.S.A., McGraw-Hill, 1964).
20. S. Hayati, K. Tso and G. Roston, "Robot Geometry Calibration," *Proceedings of the IEEE International Conference on Robotics and Automation* (1988) pp. 947–951.
21. S. A. Hayati, "Robot Arm Geometric Link Parameter Estimation," *Proceedings of the 22nd IEEE Conference on Decision and Control*, Vol. 22 (1983) pp. 1477–1483.
22. R. He, X. Li, T. Shi, B. Wu, Y. Zhao, F. Han, S. Yang, S. Huang and S. Yang, "A kinematic calibration method based on the product of exponentials formula for serial robot using position measurements," *Robotica* **33**, 1295–1313 (2015).
23. R. He, Y. Zhao, S. Yang and S. Yang, "Kinematic-parameter identification for serial-robot calibration based on poe formula," *IEEE Trans. Robot.* **26**(3), 411–423 (2010).
24. A. B. Hexagon, "Hexagon Metrology: Romer protable coordinate measuring machines," `hexagonmi.com/products/portable-measuring-arms` (2015).
25. J. M. Hollerbach and C. W. Wampler, "The calibration index and taxonomy for robot kinematic calibration methods," *Int. J. Robot. Res.* **15**(6), 573–591 (1996).
26. W. Hoppe, "Method and system to provide improved accuracies in multi-jointed robots through kinematic robot model parameters determination," US Patent 7,904,202 (2011).
27. C. Huang, C. Xie and T. Zhang, "Determination of Optimal Measurement Configurations for Robot Calibration Based on a Hybrid Optimal Method," *Proceedings of the International Conference on Information and Automation, ICIA* (2008) pp. 789–793.

https://doi.org/10.1017/S0263574718000024 Published online by Cambridge University Press

28. M. Ikits and J. M. Hollerbach, "Kinematic Calibration Using a Plane Constraint," *Proceedings of the IEEE International Conference on Robotics and Automation*, Vol. 4, (1997) pp. 3191–3196.
29. ISO/DIS 10360, "ISO/DIS 10360-12 - geometrical product specifications (gps) acceptance and reverification tests for coordinate measuring systems (cms) part 12: Articulated arm coordinate measurement machines (cmm)," Technical report, ISO (2014).
30. J. H. Jang, S. H. Kim and Y. K. Kwak, "Calibration of geometric and non-geometric errors of an industrial robot," *Robotica* **19**, 311–321 (2001).
31. W. Jing, P. Y. Tao, G. Yang and K. Shimada, "Calibration of Industry Robots with Consideration of Loading Effects Using Product-of-Exponential (poe) and Gaussian Process (gp)," *Proceedings of the IEEE International Conference on Robotics and Automation (ICRA)* (2016) pp. 4380–4385.
32. A. Joubair, M. Slamani and I. A. Bonev, "Kinematic Calibration of a Five-Bar Planar Parallel Robot Using All Working Modes," *Robot. Comput.-Integr. Manuf.* **29**(4), 15–25 (2013).
33. R. P. Judd and A. B. Knasinski, "A technique to calibrate industrial robots with experimental verification," *IEEE Trans. Robot. Autom.* **6**(1), 20–30 (1990).
34. B. Karlsson and T. Brogårdh, "A new calibration method for industrial robots," *Robotica* **19**, 691–693 (2001).
35. W. Khalil, M. Gautier and C. Enguehard, "Identifiable parameters and optimum configurations for robots calibration," *Robotica* **9**, 63–70 (1991).
36. H. O. K. Kirchner, B. Gurumoorthy and F. B. Prinz, "A perturbation approach to robot calibration," *Int. J. Robot. Res.* **6**(4), 47–59 (1987).
37. A. Knoll and P. Kovacs, "Method and device for the improvement of the pose accuracy of effectors on mechanisms and for the measurement of objects in a workspace," US Patent 6,529,852 (2003).
38. H. Larson, *Introduction to Probability Theory and Statistical Inference*. Probability and Mathematical Statistics Series. (New York, NY, U.S.A., Wiley, 1982). ISBN 9780471099192.
39. T. C. McGrath and R. B. Gilbert, "Analytical method for designing and analyzing 1d search programs," *J. Geotech. Geoenvironmental Eng.* **125**(12), 1043–1056 (1999).
40. M. A. Meggiolaro, "Manipulator Calibration Using a Single Endpoint Contact Constraint," *Proceedings of ASME Design Engineering Technical Conference* (2000).
41. S. S. Najjar, E. Shammas and M. Saad, "Updated normalized load-settlement model for full-scale footings on granular soils," *Georisk: Assess. Manage. Risk Engineered Syst. Geohazards* **8**(1), 63–80 (2014).
42. W. S. Newman and D. W. Osborn, "A New Method for Kinematic Parameter Calibration Via Laser Line Tracking," *Proceedings of the IEEE International Conference on Robotics and Automation* (1993) pp. 160–165.
43. A. Nubiola, M. Slamani, A. Joubair and I. A. Bonev, "Comparison of two calibration methods for a small industrial robot based on an optical cmm and a laser tracker," *Robotica* **32**, 447–466 (2014).
44. K. Okamura and F. Park, "Kinematic calibration using the product of exponentials formula," *Robotica* **14**, 415–421 (1996).
45. I. W. Park, B. J. Lee, S. H. Cho, Y. D. Hong and J. H. Kim, "Laser-based kinematic calibration of robot manipulator using differential kinematics," *IEEE/ASME Trans. Mechatron.* **17**(6), 1059–1067 (2012).
46. J. M. Renders, E. Rossignol, M. Becquet and R. Hanus, "Kinematic calibration and geometrical parameter identification for robots," *IEEE Trans. Robot. Autom.* **7**(6), 721–732 (1991).
47. C. Robert and G. Casella, *Monte Carlo Statistical Methods*. (New York, NY, U.S.A., Springer Science & Business Media, 2013).
48. Z. S. Roth, B. Mooring and B. Ravani, "An overview of robot calibration," *IEEE J. Robot. Autom.* **3**(5), 377–385 (1987).
49. F. Scholz, "Tolerance stack analysis methods," Technical report, The Department of Statistics at the University of Washington (1995).
50. S. Spiess, M. Vincze and M. Ayromiou, "On the calibration of a 6-d laser tracking system for dynamic robot measurements," *IEEE Trans. Instrum. Meas.* **47**(1), 270–274 (1998).
51. A. Tarantola, *Inverse Problem Theory and Methods for Model Parameter Estimation*. Other Titles in Applied Mathematics. (Philadelphia, PA, U.S.A., Society for Industrial and Applied Mathematics, 2005).
52. A. L. Welker and R. B. Gilbert, "Calibration of flow and transport model with a bench-scale prefabricated vertical drain remediation system," *J. Geotech. Geoenvironmental Eng.* **129**(1), 81–90 (2003).
53. A. L. Welker and R. B. Gilbert, "Design of a measurement program for a bench-scale pvd remediation system using Bayesian updating," *Geotech. Testing J.* **27**(3), 239–249 (2004).
54. D. Whitney, C. Lozinski and J. M. Rourke, "Industrial robot forward calibration method and results," *J. Dyn. Syst. Meas. Control* **108**(1), 1–8 (1986).
55. D. Zhang and B. Wei, "Design, analysis and modelling of a hybrid controller for serial robotic manipulators," *Robotica* **35**(9), 1888–1905 (2017).
56. H. Zhuang, Z. S. Roth and F. Hamano, "A complete and parametrically continuous kinematic model for robot manipulators," *IEEE Trans. Robot. Autom.* **8**(4), 451–463 (1992).

Appendix A: Calibration using maximum likelihood

For a pair of end-effector poses and a possible set of model parameters for the robot's forward kinematic model, one can compute the likelihood of obtaining the actual length (or error) of the artifact.

https://doi.org/10.1017/S0263574718000024 Published online by Cambridge University Press

For m measured length pairs, the likelihood function could be defined by assuming that the lengths of the artifacts for the different pairs follow a multivariate normal distribution that is defined by a mean vector and a covariance matrix thatare given by

$$\mu_{l_{ab}} = l_{ab}(\tilde{\varphi}) \text{ and} \tag{A1}$$

$$\Sigma = \text{diag}(\ldots, \sigma_i^2, \ldots) \text{ for } i = 1, 2, \ldots, m, \tag{A2}$$

where $\mu_{l_{ab}}$ is the mean vector that contains the predicted lengths from the robotic arm for all the different measurement pairs and Σ is the covariance of the predicted lengths. Implicit in the mean vector and covariance matrix are the deviations of the kinematic model parameters of the robotic arm, $\tilde{\varphi}$, and the standard deviation, σ_i, which is assumed to be a model parameter that is also determined in the calibration exercise. The standard deviation, σ_i, reflects the uncertainty in the length predictions of the robotic arm and is assumed to be a constant positive number ($\sigma_i = e^{\lambda}$ where $\lambda \in \mathbb{R}$) for all the length measurements. In addition, it is assumed that the kinematic length predictions for the different length pairs are statistically independent. This assumption leads to the diagonal covariance matrix Σ for the length measurements as indicated in (A2).

Based on the above assumptions, the likelihood function that needs to be maximized is defined by

$$\mathcal{L}(\tilde{\varphi}, \lambda) = \frac{e^{-\frac{1}{2}\left(L_{ab}-\mu_{l_{ab}}\right)\cdot\Sigma^{-1}\cdot\left(L_{ab}-\mu_{l_{ab}}\right)^T}}{(2\pi)^{m/2}\sqrt{\det\Sigma}}. \tag{A3}$$

Conventional Maximum Likelihood Estimation (MLE) methods are then used to estimate the deviations of the kinematic model parameters, $\tilde{\varphi}$, and the additional model parameter, λ, that would maximize the likelihood of obtaining the measured length data pairs, l_{ab}. The resulting MLE parameter set is obtained as

$$\left(\tilde{\varphi}^{MLE}, \lambda^{MLE}\right) = \text{argmax}\, \mathcal{L}(\tilde{\varphi}, \lambda). \tag{A4}$$

For the case where the length data is assumed to follow a multivariate normal distribution with statistically independent length measurements that have a constant standard deviation, the kinematic model parameters $\tilde{\varphi}^{reg}$ that result from minimizing the error function using regression in (8) are expected to be equivalent to the parameters $\tilde{\varphi}^{MLE}$ solved by maximizing the likelihood function in (A4). The only difference between the two approaches is the additional parameter, λ^{MLE}, which captures the uncertainty in the length measurements in the MLE method and does not play a role in the least square regression approach. The equivalence of the two approaches is proved in Appendix B.

Appendix B: Equivalence of regression and maximum likelihood methods

It should be noted that the likelihood function defined in (A3) could have been formulated in terms of the length error data rather than actual length data. In that case, the error could be defined as the difference between the actual artifact length and the length predicted by the robotic arm. Hence, the expression of the likelihood function could be modified such that

$$\mathcal{L}(\tilde{\varphi}, \lambda) = \frac{1}{(2\pi)^{m/2}\sqrt{\det\Sigma}} e^{-\frac{1}{2}Y\cdot\Sigma^{-1}\cdot Y^T}.$$

Here, Y is an error vector that contains the difference between the actual and predicted lengths, that is, $Y(\tilde{\varphi}) = \text{err}_{ab}(\tilde{\varphi}) = L_{ab} - l_{ab}(\tilde{\varphi})$.

It could also be noted that in the process of estimation of the model parameters using the method of maximum likelihood, it is more convenient to work with the natural logarithm, ln, of the likelihood function. Since Σ is a constant diagonal matrix, we have

$$\det\Sigma = \prod^{m} \sigma^2 = \sigma^{2m} = e^{2m\lambda}.$$

https://doi.org/10.1017/S0263574718000024 Published online by Cambridge University Press

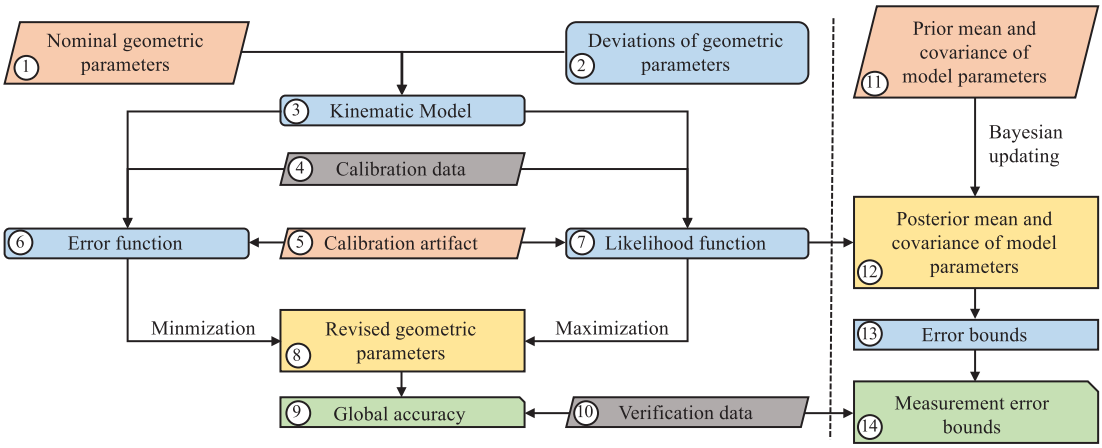

Fig. 11. The software flowchart depicted the main steps of the novel calibration approach to right of the dashed line.

Computing explicitly the ln of the likelihood function we have

$$\begin{aligned}\ell &= \ln \mathcal{L} \\ &= \ln e^{-\frac{1}{2}Y\cdot\Sigma^{-1}\cdot Y^T} - \ln\sqrt{\det\Sigma} - \ln(2\pi)^{m/2} \\ &= -\frac{1}{2}Y\cdot\Sigma^{-1}\cdot Y^T - m\lambda - \frac{m}{2}\ln(2\pi) \\ &= -\frac{1}{2}e^{2\lambda}\sum_{i=1}^{m} Y_i^2 - m\lambda - \frac{m}{2}\ln(2\pi).\end{aligned} \tag{B1}$$

From the last expression, one can clearly note that given a fixed uncertainty in the length measurements (i.e., constant λ), estimating the parameters by maximizing the likelihood function is equivalent to minimizing the RMS error of the length measurement. This can be deduced from the fact that the last two terms in (B1) are constants, that is,

$$\left(\tilde{\varphi}^{MLE} = \operatorname{argmax}\mathcal{L}(\tilde{\varphi})\right) \equiv \left(\operatorname{argmin}\mathrm{Err}(\tilde{\varphi}) = \tilde{\varphi}^{reg}\right). \tag{B2}$$

Finally, using MLE, one also estimates the variance of the length measurement uncertainty, σ which constitutes an added advantage.

Appendix C: Raw data

In this section, a flowchart depicting the major blocks of the software which were used to implement the novel calibration method is depicted in Fig. 11. It is worth noting that all computations and most figures we produced using a commercially available software, Mathematica®. The artifact data and the raw encoder data that was used in this paper are included in Table VII. The second row of Table VII depicts the three-dimensional locations of the six holes on the used artifact. One can compute the actual length between any two pair of holes using the following equation $l_{ij} = \sqrt{(p_i - p_j)^T(p_i - p_j)}$. Note that, since the artifact has a total of six points, one can compute up to 15 lengths from all possible unique pair or points. In fact, these lengths attributes of the artifact are depicted in *Block 5* in Fig. 11. Moreover, 10 of these lengths were used for calibration, *Block 4* while five of these lengths were used for verification, *Block 10*.

Additionally, the second portion of Table VII includes the raw encoder angles, in degrees, for all the measurements done with the system. For each row of the angle data, the artifact was held rigidly with respect to the base of the manipulator and the end-effector was placed in all six holes on the artifact in the correct sequence. Accordingly, starting with nominal geometric parameters, *Block 1*,

https://doi.org/10.1017/S0263574718000024 Published online by Cambridge University Press

Table VII. The three-dimensional location of the six holes on the artifact (mm) and the raw encoder angles for all the measured configuration (Degrees).

Point 1			Point 2			Point 3			Point 4			Point 5			Point 6		
x_1	y_1	z_1	x_2	y_2	z_2	x_3	y_3	z_3	x_4	y_4	z_4	x_5	y_5	z_5	x_6	y_6	z_6
40.609	133.038	9.365	232.819	119.738	9.429	542.214	91.415	9.638	35.226	69.608	9.424	223.947	42.366	9.541	536.528	19.801	9.634
η_1^1	η_2^1	η_3^1	η_1^2	η_2^2	η_3^2	η_1^3	η_2^3	η_3^3	η_1^4	η_2^4	η_3^4	η_1^5	η_2^5	η_3^5	η_1^6	η_2^6	η_3^6
255.78	53.46	73.62	211.32	55.26	88.92	157.14	54.54	62.10	249.66	54.72	63.00	214.38	53.28	76.68	166.50	57.96	48.24
97.02	−157.68	−70.02	62.82	−159.66	−85.50	−4.68	−158.76	−58.68	87.66	−158.94	−59.58	56.70	−157.50	−73.26	1.62	−162.36	−44.82
172.44	53.10	72.54	128.52	55.62	90.72	67.50	53.28	69.12	165.96	54.36	62.64	130.32	52.92	79.38	77.58	55.26	57.42
12.78	−157.50	−69.12	−16.74	−160.02	−87.30	−92.88	−157.50	−65.70	3.24	−158.58	−59.22	−25.56	−157.32	−75.96	−85.32	−159.66	−54.00
78.12	52.92	79.02	27.18	57.06	93.06	−27.90	54.18	64.98	71.28	53.10	70.20	31.86	53.28	82.62	−17.64	56.70	53.64
284.76	−157.14	−75.42	248.40	−161.64	−89.64	172.80	−158.58	−61.74	273.96	−157.50	−66.78	240.48	−157.68	−79.20	180.72	−160.92	−50.22
−18.90	53.28	77.40	−67.14	55.62	89.28	−116.28	56.16	56.16	−24.66	53.82	67.14	−61.74	53.46	77.04	−106.92	60.84	40.86
186.12	−157.50	−73.98	147.78	−160.02	−85.86	82.62	−160.56	−52.74	176.76	−158.22	−63.72	143.28	−157.68	−73.62	89.82	−165.06	−37.44
101.88	−73.62	−100.08	77.76	−51.84	−126.54	9.00	−64.26	−112.32	93.78	−81.00	−89.46	69.48	−65.70	−110.88	14.58	−73.80	−99.54
264.78	−30.24	103.68	231.48	−52.02	129.96	169.02	−39.60	115.74	258.84	−22.86	92.88	229.86	−38.16	114.48	178.20	−30.06	102.96
180.54	−29.16	101.52	149.40	−54.54	132.12	76.68	−47.34	124.56	173.88	−22.68	91.98	145.44	−41.22	117.72	86.94	−37.08	112.32
19.80	−74.88	−98.10	0.00	−49.32	−128.52	−75.96	−56.52	−121.14	11.52	−81.18	−88.56	−10.08	−62.64	−114.12	−69.84	−66.78	−108.90
−273.78	−33.30	107.10	−308.34	−58.14	135.36	−18.36	−44.46	121.68	79.02	−26.64	97.56	48.24	−43.74	120.60	−7.92	−34.92	109.98
286.56	−70.74	−103.50	263.70	−45.72	−131.76	186.12	−59.40	−118.26	277.56	−77.40	−94.14	253.08	−60.12	−117.18	192.96	−68.94	−106.56
−10.26	−33.84	108.18	−46.44	−54.90	132.84	−108.00	−37.98	114.12	−16.20	−26.28	97.74	−46.98	−40.50	117.18	−98.64	−28.80	101.70
190.08	−70.20	−104.76	163.62	−48.96	−129.24	93.60	−65.88	−110.70	181.98	−77.58	−94.32	155.70	−63.36	−113.76	99.90	−75.06	−98.28
49.50	−42.12	−134.10	14.40	−80.64	−127.62	−13.50	−136.62	−66.60	47.16	−55.62	−121.68	20.70	−86.76	−113.76	−6.48	−141.12	−54.18
197.64	−61.56	137.70	169.56	−23.40	131.22	151.74	32.40	70.20	203.58	−48.24	125.28	181.26	−17.10	117.36	160.02	36.90	57.78
−23.76	−36.54	−138.06	−64.98	−76.68	−135.90	−99.72	−133.02	−78.66	−29.52	−51.12	−125.82	−59.58	−82.80	−121.68	−92.16	−136.08	−68.22
−243.18	−67.32	141.66	−278.10	−27.36	139.50	−298.62	28.98	82.08	−238.68	−52.74	129.42	−265.14	−21.24	125.28	−289.44	32.04	71.82
−116.82	−27.54	−143.64	−164.34	−75.42	−140.04	−198.00	−133.20	−79.92	−124.02	−44.64	−131.94	−156.96	−80.82	−126.72	−189.72	−135.72	−71.10
15.48	−76.32	147.24	−20.34	−28.44	143.64	−37.08	29.16	83.52	22.32	−59.22	135.54	−4.68	−23.22	130.50	−27.36	31.50	74.70
136.44	−41.76	−134.46	102.24	−81.72	−126.18	75.42	−138.24	−62.82	135.36	−55.26	−122.22	109.44	−87.66	−112.86	82.62	−143.10	−50.22
−78.48	−61.92	138.06	−104.58	−22.32	129.78	−120.60	34.20	66.42	−71.28	−48.60	125.82	−92.70	−16.38	116.46	−112.32	38.70	53.82
200.52	26.28	111.24	176.22	−2.34	118.44	157.86	−14.76	78.12	205.38	25.92	99.72	185.76	2.34	103.86	165.42	−6.66	64.44
46.44	−130.50	−107.64	17.46	−101.70	−114.84	−8.46	−89.28	−74.52	45.54	−130.14	−96.12	22.68	−106.38	−100.26	−2.34	−97.38	−60.84
115.38	27.36	116.46	85.68	−4.32	127.44	65.16	−22.68	90.54	119.70	25.38	106.02	96.66	−1.08	113.40	73.62	−15.48	79.02
−33.30	−131.76	−113.04	−68.40	−99.72	−124.02	−99.90	−81.18	−86.94	−36.72	−129.60	−102.42	−63.18	−102.96	−109.80	−92.88	−88.38	−75.42

Table VII. Continued.

Point 1			Point 2			Point 3			Point 4			Point 5			Point 6		
x_1	y_1	z_1	x_2	y_2	z_2	x_3	y_3	z_3	x_4	y_4	z_4	x_5	y_5	z_5	x_6	y_6	z_6
14.40	30.60	122.22	−16.20	−4.32	132.30	−32.94	−23.58	92.52	21.42	26.46	112.86	−2.52	−2.34	119.88	−23.94	−17.46	82.98
−126.90	−135.00	−118.62	−167.94	−99.72	−128.88	−198.54	−80.28	−88.92	−130.86	−130.68	−109.44	−160.74	−101.70	−116.28	−190.80	−86.40	−79.38
−77.22	27.72	115.56	−101.70	−2.70	121.32	−117.54	−14.58	78.48	−70.38	25.92	105.12	−90.54	1.08	108.00	−109.62	−7.38	66.42
−227.52	−131.94	−111.96	−259.20	−101.34	−117.90	−284.58	−89.28	−74.88	−227.70	−130.14	−101.52	−252.18	−105.12	−104.58	−277.92	−96.66	−62.82
−149.94	52.20	54.18	−150.30	15.30	88.20	−149.58	−27.18	90.00	−141.12	52.38	53.64	−139.32	16.02	87.30	−139.68	−26.82	89.46
−315.36	−156.42	−50.58	−315.54	−119.52	−84.60	−315.00	−76.68	−86.40	−306.36	−156.60	−50.22	−304.56	−120.06	−83.70	−304.92	−77.22	−85.86
−0.54	−152.46	−65.52	−0.72	−115.20	−97.74	−0.18	−66.78	−99.54	8.82	−152.82	−64.44	10.80	−116.10	−95.94	10.26	−67.86	−98.10
−201.24	48.24	69.12	−201.60	11.16	101.16	−200.88	−37.08	102.96	−190.80	48.60	67.86	−189.00	12.06	99.36	−189.18	−36.00	101.52
−86.04	−153.00	−62.82	−86.40	−115.92	−95.22	−86.04	−68.58	−97.02	−75.96	−153.00	−62.46	−74.16	−116.46	−94.14	−74.88	−69.12	−96.30
76.86	48.78	66.42	76.32	11.88	98.64	76.68	−35.28	100.62	86.76	48.78	65.88	88.56	12.42	97.74	88.02	−34.74	99.90
−327.42	48.42	67.86	−328.14	11.52	100.08	−327.78	−36.18	101.88	−317.16	48.60	66.78	−315.54	12.24	98.46	−316.26	−35.28	100.62
−127.26	−152.82	−64.26	−127.62	−115.56	−96.48	−127.62	−67.68	−98.28	−117.36	−153.00	−63.36	−115.56	−116.46	−94.86	−116.46	−68.58	−97.02
−3.60	48.78	67.68	−4.32	11.70	99.90	−3.96	−35.82	101.52	5.76	49.32	65.16	7.38	12.96	96.66	6.48	−33.84	98.82
195.84	−153.00	−64.08	195.48	−115.92	−96.30	195.48	−68.22	−98.10	205.56	−153.54	−61.56	207.00	−117.00	−93.06	206.10	−70.20	−95.22
−105.30	50.94	59.04	−105.66	14.22	92.34	−105.12	−29.88	93.96	−95.94	51.30	57.60	−94.14	15.12	90.36	−94.50	−28.80	92.52
93.42	−155.16	−55.44	93.06	−118.26	−88.74	93.42	−73.98	−90.54	102.60	−155.70	−54.18	104.40	−119.16	−86.76	103.68	−75.06	−88.92

one could use the raw angles of each row to compute six three-dimensional positions through the forward kinematics, *Block 3*, of the manipulator. Then using the computed positions of the artifact, one can compute lengths using pairs of points. Comparing the computed lengths to the actual lengths of the artifact, one can construct either an error function, *Block 6*, or a likelihood function, *Block 7*. Minimizing the error or maximizing the likelihood function equivalently solves for the deviations of the geometric parameters, *Block 2*, which in turn can be used to revise the nominal parameters, *Block 8*. Using the verification data, *Block 10* and the revised set of parameters, one can estimate the global accuracy of the robotic arm, *Block 9*.

Finally, for the novel proposed method, starting with prior model parameters, *Block 11*, and the likelihood function, *Block 7*, one can compute the posterior model parameters, *Block 12*, by using Bayesian updating. Using the posterior model parameters, error bound can be computed for all measurement, *Blocks 13 and 14*.

https://doi.org/10.1017/S0263574718000024 Published online by Cambridge University Press